NASA TECHNICAL NOTE

NASA TN D-3792

NASA TN D-3792

MECHANICAL ABSORPTION OF ACOUSTIC OSCILLATIONS IN SIMULATED ROCKET COMBUSTION CHAMBERS

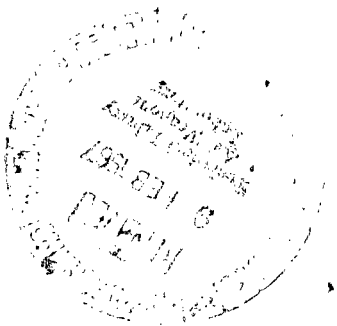

by Bert Phillips and C. Joe Morgan, Joseph C. Kauffman

Lewis Research Center
Cleveland, Ohio

NATIONAL AERONAUTICS AND SPACE ADMINISTRATION • WASHINGTON, D. C. • JANUARY 1967

ERRATA

NASA Technical Note D-3792

MECHANICAL ABSORPTION OF ACOUSTIC OSCILLATIONS IN SIMULATED ROCKET COMBUSTION CHAMBERS

by Bert Phillips and C. Joe Morgan

January 1967

Page 5: Equation (8) should read

$$p = \frac{2\bar{K}\psi\omega}{\left[4\omega_n^2 k_n^2 + \left(\omega^2 - \omega_n^2\right)^2\right]^{1/2}}$$

Page 27: The equation in line 23 should read

$$\pi\left|\Delta f\right| = k_n$$

Page 47: Equation (D11) should read

$$X = \frac{2\pi f_0 l_{eff}}{c\sigma}\left(\frac{f}{f_0} - \frac{f_0}{f}\right)$$

Corrected 10 Jan 68
Lab

NASA-Langley, 1967

Issued 12-7-67

Completed 18 June 68-SJ

ERRATA 2

NASA Technical Note D-3792

MECHANICAL ABSORPTION OF ACOUSTIC OSCILLATIONS IN SIMULATED ROCKET COMBUSTION CHAMBERS

by Bert Phillips and C. Joe Morgan

January 1967

Cover, title page, page 1: The authorship of the report should include Joseph C. Kauffman as third author.

Issued 5-3-68

NASA TN D-3792

MECHANICAL ABSORPTION OF ACOUSTIC OSCILLATIONS IN SIMULATED ROCKET COMBUSTION CHAMBERS

By Bert Phillips and C. Joe Morgan, Joseph C. Kauffman

Lewis Research Center
Cleveland, Ohio

NATIONAL AERONAUTICS AND SPACE ADMINISTRATION

For sale by the Clearinghouse for Federal Scientific and Technical Information
Springfield, Virginia 22151 – Price $2.00

CONTENTS

MECHANICAL ABSORPTION OF ACOUSTIC OSCILLATIONS IN SIMULATED ROCKET COMBUSTION CHAMBERS

by Bert Phillips and C. Joe Morgan, Joseph C. Kauffman

Lewis Research Center

SUMMARY

Resonant absorbers to damp combustion oscillations in rocket motors were simulated by cold-flow tests. Acoustic waves were used to evaluate single Helmholtz resonators and perforated liners in a cylindrical test chamber. The first standing and spinning tangential, second standing tangential, and first radial were the wave modes tested. The geometrical parameters studied were liner-hole diameter, liner thickness, liner-back distance, and partitions in the liner-back space. In addition, the effects on damping of mean flow past the liner, high wave amplitude, wave frequency, and the angle of incidence between the wave and the axis of the liner hole were evaluated.

The damping devices were mounted in the cylindrical test cavity. The damping coefficients of the standing waves were measured by both transient and steady-state techniques and then compared with results from a set of theoretical and empirical equations. These equations were based on the assumption that a perforated liner behaves as an array of Helmholtz resonators. There was no quantitative correlation between the experimental and theoretical results; the trends in damping caused by changes in geometrical and wave parameters, however, were generally predictable. The results that did not compare qualitatively with theoretical predictions involved frequency - hole spacing - flow velocity interactions, increase in tangential mode damping with longitudinal partitioning of the liner-back space, and absorption of resonators with an angle of incidence other than 0^{o} between wave direction and resonator neck.

The perforated liners were equally effective in damping both spinning and standing tangential waves. In addition, it was indicated that a liner could operate effectively over a wide range of conditions if it were provided with a range of hole sizes.

INTRODUCTION

Screech or high-frequency combustion instability has been a limiting factor in the development of large rocket combustors. The excessive heat transfer and vibration associated with the pressure oscillations frequently lead to thermal or mechanical failure of the combustor (ref. 1). It is, therefore, essential that a means of minimizing or eliminating these oscillations be found.

One approach is to increase the wave damping within the combustion chamber by perforated liners on the chamber walls. These liners are thin shells that match the internal contours of the combustion chamber with a small gap between the shell and the inside wall of the chamber. The perforations are generally round holes that are arranged in a uniform array and that cover the entire surface of the liner. Perforated liners are known to be effective in suppressing oscillations in ramjet combustors (ref. 2). Accordingly, a set of equations has been obtained from references 3 to 5 for the design of an acoustic liner for a rocket combustor.

The use of the equations is limited because of the experimental method employed in references 3 to 5. The method involves measurements in an impedance tube with normal incidence of the wave on the absorber. The cylindrical shape of rocket chambers, however, gives rise to pressure oscillations that are generally tangential to the chamber walls (ref. 1). The angle of incidence between wave direction and resonator surface is no longer normal, and, since reference 4 predicts that the angle of incidence has a strong effect on absorption, the impedance tube results may not be valid for the cylindrical shape. In addition, the relation between results in an impedance tube and in a resonant cavity with damping on the walls (i.e., the rocket combustion chamber) has not been completely established for standing waves in the cavity (ref. 6).

The limitations on the use of the equations from references 3 to 5 for designing a rocket-engine liner necessitated a bench-type evaluation of damping devices in a simulated system. The complete simulation of rocket conditions in the bench system was not possible because of the absence of two-phase flows, transport processes, and the intense heat that is characteristic of rocket combustors. In addition, the pressure oscillations during screech are nonsinusoidal, vary in frequency, and can exceed the mean chamber pressure in amplitude. The bench test facility, however, used ambient-temperature air as a medium for wave transmission, and the maximum amplitude of the acoustic oscillations was well below ambient pressure. Nonetheless, the effects on damping of cylindrical cavity geometry, absorber geometry, and mean flow past the liner could be determined and the design equations evaluated under these conditions. The maximum amplitude of the acoustic oscillations was 170 decibels (ref. to 10^{-4} μbar), which is well into the nonlinear range of the resonant absorbers tested, so that effects of high wave amplitude could be determined and extrapolated to screech conditions.

Two general types of damping devices were studied herein, the perforated liners previously mentioned and individual resonant absorbers. The individual or single resonators were cavities with adjustable volumes and small openings that could be mounted easily on the test chamber wall. The purpose of testing single resonators was to provide data on conditions between those of references 3 to 5 and the perforated liners of this investigation.

Four types of cylindrical acoustic modes were used to evaluate the absorbers: the first tangential mode, the second tangential mode, the first spinning tangential mode, and the first radial mode. The modes were excited by sound driver units (ref. 7), and the sound pressure level was measured by probe microphones.

Three kinds of data were taken to determine the absorption of a damping device: the reduction of the steady-state sound pressure level at a pressure antinode, the decay rate of a wave measured at a pressure antinode when the driver or drivers were turned off, and the frequency bandwidth of the modal peak. These data were converted into damping coefficients and compared with one another and with the damping predicted by the equations of references 3 to 5.

The measurements for no mean flow past the absorber were taken with the absorber mounted in a cylindrical test chamber closed at both ends. Measurements with mean flow were taken by making the test chamber with absorber an integral part of a wind tunnel. The flow past the liner was ambient-temperature air. The wind tunnel was approximately constant in diameter, and no attempt was made to simulate a sonic nozzle.

The following range of parameters was studied:

Liner thickness, in.	1/16 to 3/4
Single resonator neck length, in.	0.172 to 0.766
Perforation or hole diameter, in.	5/32 to 7/16
Hole spacing, in.	1/2 and 1
Mean flow velocity past liner, ft/sec	0 to 159
Sound pressure level, dB referenced to 2×10^{-4} μbar	up to 170
Wave frequency, Hz	800 to 2100
Resonator or liner-back space, in.	1/16 to 3/4
Angle of incidence, deg	45 to 90

Back space partitions were circumferential, axial, and combined.

THEORY

Liner-Design Equations

An acoustic liner with circular holes for perforations is shown in figure 1(a). In

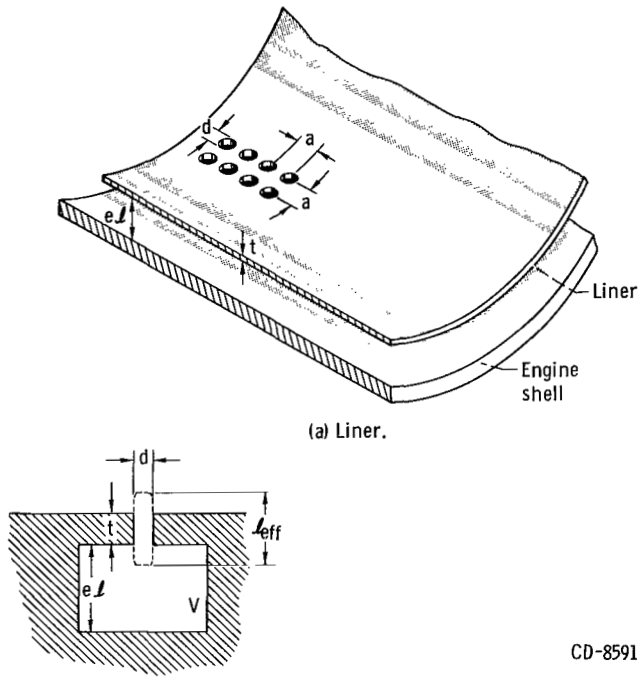

Figure 1. - Schematic illustration of acoustic liner and single resonator cross sections.

figure 1(b) is shown a schematic drawing of a single resonator. The following equations are applicable to either device. (All symbols are defined in appendix A.)

Open area ratio (ref. 4):

$$\sigma = \frac{\pi}{4}\frac{d^2}{a^2} = \frac{(A)e\ell}{V} \tag{1}$$

where A is the perforation area, V is the resonant cavity volume for one perforation, and $e\ell$ is the height of the liner gap.

Effective liner thickness (ref. 4):

$$\ell_{eff} = t + 0.85d\left(1 - 0.7\sqrt{\sigma}\right) \tag{2}$$

Liner resonant frequency (ref. 3):

$$f_0 = \frac{c}{2\pi}\sqrt{\frac{\sigma}{(e\ell)\ell_{eff}}} \tag{3}$$

where c is the sonic velocity of the gas behind the liner.

Resonant frequency of single resonator (ref. 3):

$$f_0 = \frac{c}{2\pi}\sqrt{\frac{A}{V\ell_{eff}}} \tag{4}$$

Liner acoustic reactance (ref. 4):

$$X = \frac{2\pi f_0 \ell_{eff}}{c\sigma}\left(\frac{f}{f_0} - \frac{f_0}{f}\right) \tag{5}$$

where f is the input wave frequency, and, if $f = f_0$, $X = 0$.
Liner acoustic resistance (ref. 3):

$$\theta = \frac{4(\pi\mu\rho f)^{1/2}}{\sigma\rho c}\left(\epsilon + \frac{t}{d}\right) \tag{6}$$

where ρ is the density of the gas in the resonator neck, μ is the shear viscosity of the gas in the neck, and ϵ is a nonlinear wave amplitude correction factor.
Ratio of absorbed to incident acoustic intensity (ref. 4):

$$\alpha = \frac{4\theta}{(\theta + 1)^2 + X^2} \tag{7}$$

where ℓ_{eff} and θ are functions of mean flow past the absorber, as defined in reference 5. The nonlinear wave amplitude correction factor ϵ is a function of the frequency f and the wave amplitude, as defined in reference 3. Consequently, α is a function of mean flow and wave amplitude. A more detailed discussion of the liner-design equations is found in appendix B.

Damping Coefficient Theory

Acoustic pressure at any point in a cavity (ref. 8) is defined by

$$p = \frac{2\bar{K}\psi}{\left[4\omega_n^2 k_n^2 + \left(\omega^2 - \omega_n^2\right)^2\right]^{1/2}} \tag{8}$$

See Errata

where ψ is the acoustic potential defined by $J_n(\omega_r r/c)\cos n\zeta \cos \omega\tau$, $\overline{K}$ is the acoustic driver source strength independent of frequency, k_n is the damping coefficient of the n^{th} mode, ω is the input angular frequency, and ω_n is the angular frequency of the n^{th} mode. Equation (8) is an expression for the acoustic pressure at any point in a cylindrical cavity, which is excited by an acoustic source at the cavity wall. If a resonant absorber is placed within the cavity, the k_n will be altered and generally increased. In this report, the effectiveness of an acoustic absorber will be measured by the change in k_n. This change in k_n is determined by the following:

(1) Changes in the sound pressure level:

If $\omega = \omega_n$,

$$p = \frac{\overline{K}}{k_n}\psi = p_{max}\psi$$

Therefore,

$$k_n \propto \frac{1}{p}$$

(2) Decay rate of the n^{th} mode:

If the source is turned off at $\tau = 0$, then, for any point in the cavity,

$$p = p_{max}\exp(-k_n\tau)$$

Therefore, k_n is the exponential decay rate of p.

(3) *Modal bandwidth:*

If $p/p_{max} = \sqrt{2}/2$, then, for ω_1 and ω_2 corresponding to $p/p_{max} = \sqrt{2}/2$,

$$k_n = \frac{1}{2}|\omega_1 - \omega_2|$$

The bandwidth of the modal peak is $|\omega_1 - \omega_2| = 2\pi|f_1 - f_2| = 2\pi|\Delta f|$, and the three preceding determinations of k_n are analytical expressions that show how these changes in k_n are measured.

Cylindrical Acoustic Modes

The characteristic pressure profiles of the acoustic modes tested in this experiment are presented in appendix C. For this experiment, the first tangential mode was at

approximately 900 hertz, the first radial mode was at approximately 1900 hertz, and the second tangential mode was at approximately 1300 hertz.

APPARATUS

Test Chamber

The bare test chamber is shown in figure 2(a). The chamber inside diameter was 10.85 inches, and the aluminum walls were 1/2 inch thick. The overall length of 17.25 inches included a 4-inch-long rotatable section near the middle for circumferential variation of microphone or resonator position relative to the driver. There were eight access ports in the test chamber, four in the rotating section and four in the adjacent fixed section. The four ports were spaced at 90° intervals on the circumference and provided for insertion of either sound drivers, resonators, or microphones.

With an acoustic liner installed (fig. 2(b)), the inside diameter was reduced to 8.85 inches and, when the ends were closed by 1/2-inch-thick aluminum plates, the internal length of the test chamber was 12.5 inches. Since the interior of the test chamber was fixed at 10.85 inches in diameter and the liner inside diameter was fixed at 8.85 inches, there was a distance of 1 inch available for the sum of both liner thickness and liner-gap height. In order to vary the liner-gap height or back distance without changing the liner thickness, it was necessary to insert a series of concentric shells between the liner and the test chamber inside wall. The space between the liner and the inside of the cylindrical shell then served as the back distance.

For flow testing, the liner was mounted in a wind tunnel with wood fairings installed to ensure a smooth flow transition to the liner surface (fig. 3). Air was driven through the tunnel by a continuously evacuated surge tank; flow was controlled by the operation of upstream and downstream butterfly valves (fig. 4). For minimum turbulence, a flat velocity profile, and maximum acoustic isolation of the test section from the rest of the tunnel, two 7-mesh screens were installed, one upstream and one downstream. The inlet and outlet sections of the tunnel were wire-reinforced rubber to minimize propagation of vibration along the tunnel walls. The flow was subsonic for the entire length of the tunnel for all flow conditions.

For excitation of the acoustic modes, either one or two drivers were used. For testing with no mean flow past the liner and for higher precision testing in the wind tunnel, electrical drivers were used. For tests with the liner mounted in the wind tunnel, where high amplitudes were required, electropneumatic drivers were used. Figure 5 (p. 10) shows the relation between the position of the driver or drivers and the acoustic field of the mode. Of the four modes tested, only the first spinning tangential mode

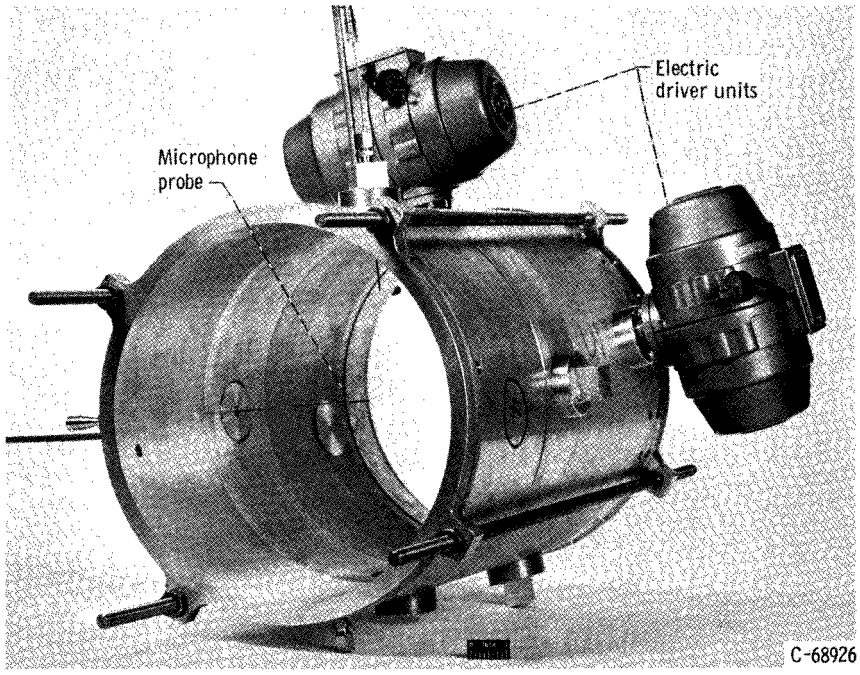

(a) Without acoustic liner.

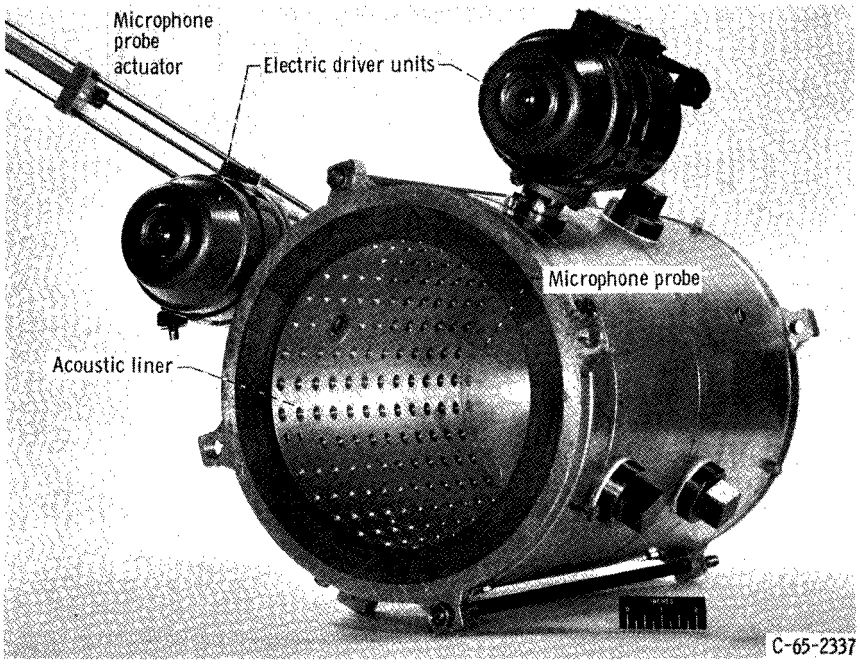

(b) With acoustic liner.

Figure 2. - Test section.

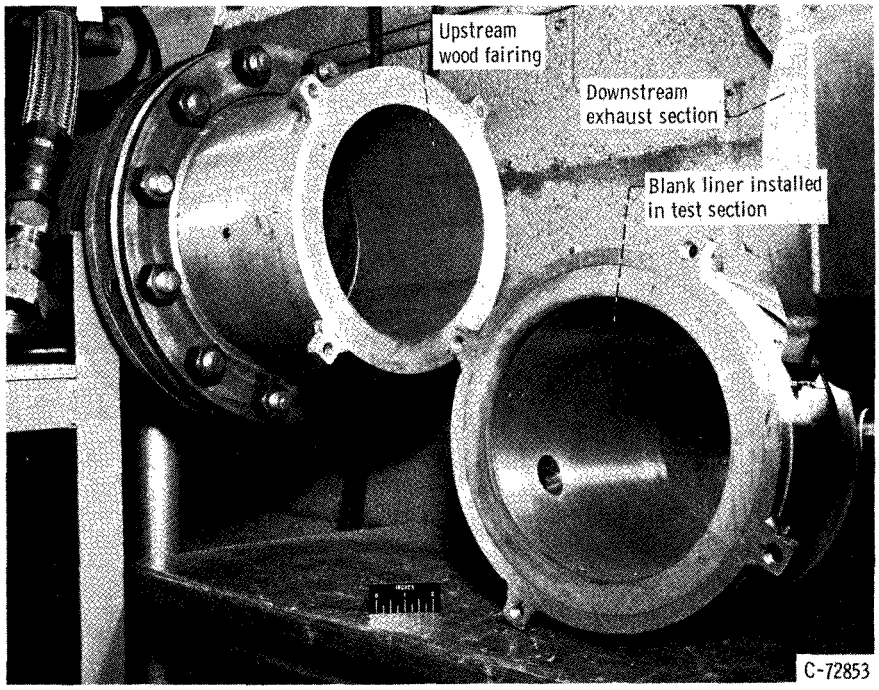

Figure 3. - Tunnel with blank liner test section removed. Flow from left to right.

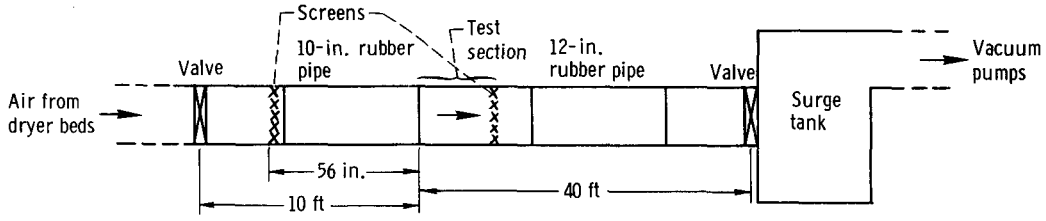

(a) Tunnel test system.

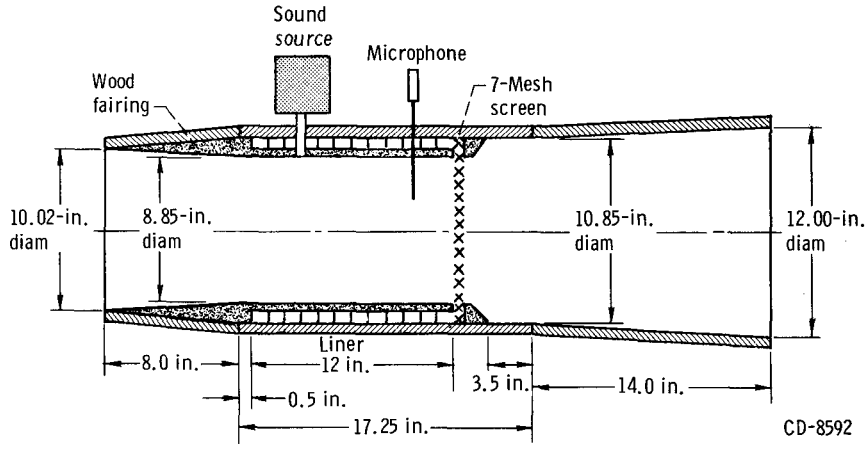

(b) Tunnel test section.

Figure 4. - Schematic illustration of tunnel test section and system.

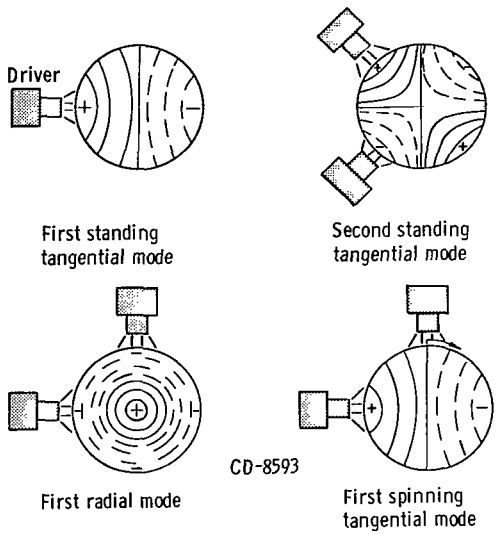

Figure 5. - Cross section of test chamber showing isobars and driver positions.

required two drivers to excite it, but two drivers were also used for the radial and second tangential modes for increased wave amplitude. Figure 6 is a block diagram of the electrical circuitry used for both electrical and electropneumatic drivers. The frequency oscillator is the source of the oscillations for the drivers. The frequency oscillator could have either a single-frequency output or a random-noise output, that is, random from 0 to 20 000 hertz. For a single-frequency output, the frequency could be controlled to within 1 hertz over the range 10 to 10 000 hertz. The phase shifter was used to shift the signal to one of the drivers by 90^{o} when the first spinning tangential mode was to be tested. The voltmeter

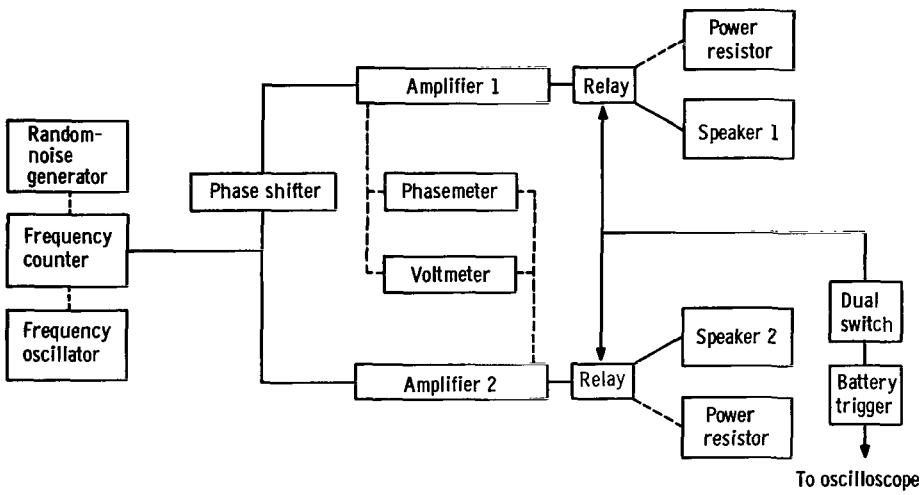

Figure 6. - Electrical circuitry for electrical and electropneumatic drivers.

and phasemeter were used to ensure the proper relation between the two signals. For decay-rate measurements, an electrical signal from the oscilloscope turned off both drivers simultaneously by shunting the amplified signals to power resistors.

In order to decouple the driver from the chamber and to make the input wave amplitude independent of the frequency, a high acoustic resistance was placed between the driver and the chamber (ref. 8). This high resistance consisted of several bare copper wires that fit within a tubular connector and transformed it into a multiple capillary tube. Repeated observations showed that the tubular connector alone, without the wires, provided a sufficient acoustic resistance to render the driver input insensitive to frequency,

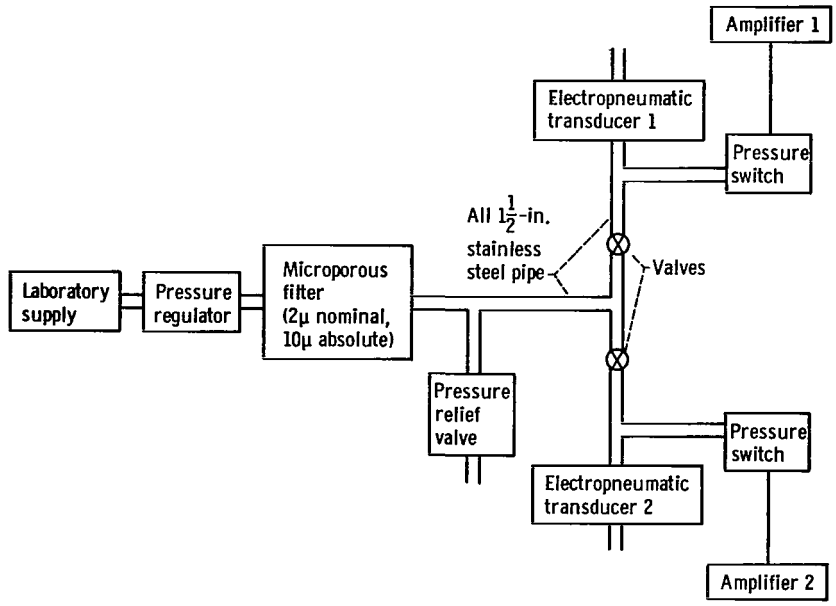

Figure 7. - Pneumatic input for electropneumatic transducers.

and the wires were eliminated. These tubular connectors were 3/8 inch in inside diameter for the electrical drivers and 7/8 inch for the electropneumatic drivers.

Figure 7 is a block diagram of the pneumatic input for the electropneumatic drivers. Each driver operated with 300 standard cubic feet per minute of air and was rated at an acoustic output of 2000 watts. For decay-rate measurements, only the electrical signal was turned off; the flow remained.

Probe-type microphones were used for examination of the acoustic field within the test chamber. The probe was a 0.04-inch-inside-diameter tube, approximately 6 inches long, attached to a 1/4-inch microphone. It was necessary to examine the internal field in order to identify the mode by its pressure profile. Figure 8 is the block diagram of the sound-analysis circuitry for both steady-state and transient measurements. The X, Y-plotter was used for recording the steady-state cross-section pressure profiles, decay rates were obtained by photographing the trace on an oscilloscope screen, and the

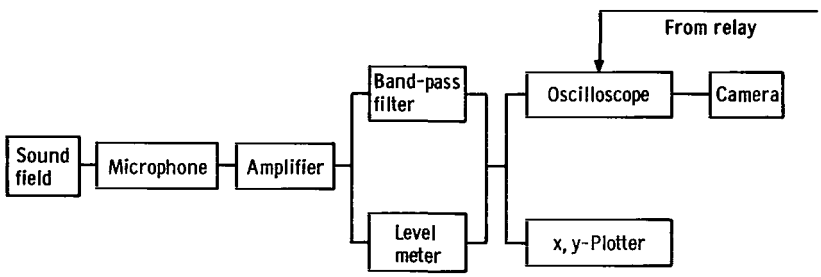

Figure 8. - Sound-analysis circuitry for steady-state and transient measurements.

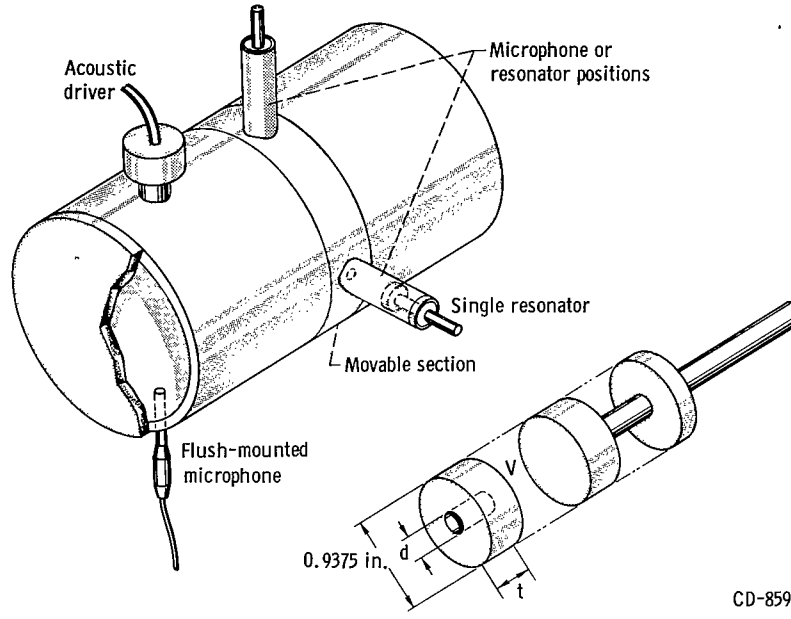

(a) Mounted on test chamber.

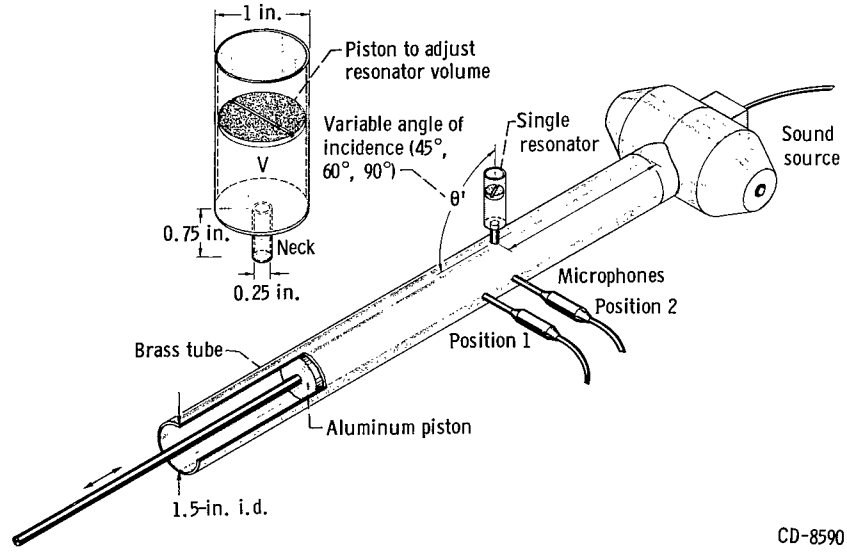

(b) Mounted on resonance tube.

Figure 9. - Schematic illustrations of single resonator.

TABLE I. - FIXED DIMENSIONS OF SINGLE RESONATORS EVALUATED ON TEST CHAMBER

Configuration	Neck length, t, in.	Neck diameter, d, in.
1	0.766	0.3125
2	.617	↓
3	.453	
4	.672	
5	.266	
6	.172	
7	.406	.2185

TABLE II. - PARAMETERS VARIED IN PERFORATED ACOUSTIC LINER EXPERIMENTS

[WO, without partitions; W, with circumferential and axial partitions; W, WO, with and without circumferential and axial partitions.]

Liner thickness, t, in.	Hole spacing, a, in.					
	1/2			1		
	Liner hole diameter, d, in.					
	5/32	3/16	7/32	5/16	3/8	7/16
0.75	WO	WO	W, WO	W, WO	W, WO	W, WO
.665				W[a]		
.60				W[a]		
.45			W[a]	W, WO[a]	W[a]	W[a]
.25				WO[b]	WO[a]	WO[a]
.0625				WO[a]		

[a]Tested with mean flow past liner.

[b]Tested with mean flow past liner and also with no mean flow and with liner backing distances of 0.16, 0.27, 0.435, 0.65, and 0.75 in.

narrow band pass filter was used to reduce the noise level in the input signal.

Single Resonator

Figure 9(a) is a detailed drawing of a single resonator showing the positions in which the resonator could be mounted on the test section. The resonators were 0.9375-inch-inside-diameter cylindrical tubes within which a piston could slide. At one end was a plug of a thickness corresponding to the neck length t and with a hole or neck diameter d. The cavity volume V was adjusted by moving the piston. The fixed dimensions of the resonators that were tested to vary neck length, as in figure 9(a), are shown in table I.

Figure 9(b) shows the apparatus used for variation of the angle of incidence between the wave direction and the resonator neck. A single resonator, the dimensions of which are given in figure 9 (p. 12), was attached approximately 1 foot from the sound driver and exactly between two microphones. The microphones were flush mounted with the inside of the brass tube. The resonant length of the tube could be changed by moving the tube piston.

Acoustic Liners

The parameters tested in the perforated acoustic liner experiments are given in table II. Figure 10 shows an

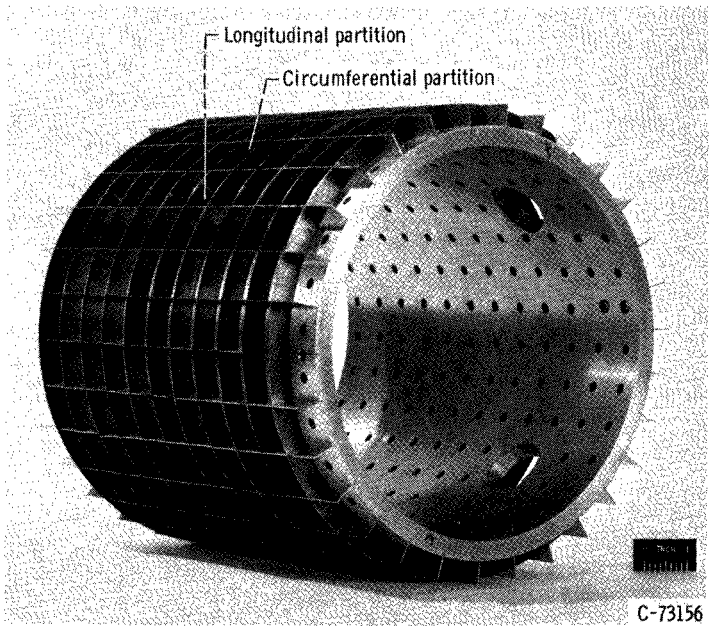

Figure 10. - Perforated acoustic liner with partitions.

acoustic liner with both circumferential and longitudinal partitions prior to insertion into the test chamber. The liner could be tested with circumferential, longitudinal, or both sets of partitions.

PROCEDURE

Frequency Response of Closed-End Solid-Wall Test Chamber

The chamber was assembled with a blank or unperforated liner and closed ends. One electrical speaker was used. The position of the microphone probe was at the wall opposite the speaker for the frequency range 400 to 1600 hertz (tangential modes) and at the centerline of the test chamber for frequencies above 1600 hertz (radial modes). Initially, the amplitude response of the chamber was plotted for the range 400 to 2100 hertz. The peaks in the response curve that corresponded to the theoretical modal frequencies were tentatively called the modal peaks. The spatial pressure fields that were set up by tuning the driver to the modal peaks were then probed radially and circumferentially to verify the identity of the modes.

Response of Closed-End Test Chamber to Random-Noise Input

The purpose of the following test was to simulate the response of a combustor to combustion noise. The chamber was set up in the same manner as was previously described herein but with the random-noise generator connected to the input terminals instead of to the single-frequency oscillator. The narrow-band pass filter with a 40-decibel-per-octave characteristic was used, and the center frequency of the filter was varied from 400 to 2100 hertz to provide a frequency scan of the chamber response to the random noise.

Tests With Angle-of-Incidence Apparatus With Single Resonator

In order to determine the effect of the angle of incidence between the neck of the resonator and the wave vector on resonator damping, the apparatus was assembled with the neck angle at 45°, 60°, or 90° (see fig. 9(b), p. 12). The speaker was tuned to a frequency corresponding to the first longitudinal mode, and the resonator was at a point midway between a node and an antinode. The microphones at positions 1 and 2 were used to ensure that the mode was correctly established with respect to the resonator position. The resonator volume was then tuned to give maximum damping, and the sound pressure level was recorded from microphone 1. This procedure was repeated for all three neck angles.

Tests With Single Resonator Mounted on Closed-End Test Chamber

Determination of effect of circumferential position variation. - A single resonator (configuration 7, table I, p. 13) was inserted into the wall of the test section. The speaker was tuned to the first standing tangential mode, and the resonator cavity volume was adjusted to give maximum damping in the test section (i.e., the sound level at a pressure antinode was minimized). The single resonator was then shifted circumferentially in increments of 10° and the microphone, which remained opposite the speaker at the antinode, recorded the sound level within the chamber at each increment.

Determination of effect of resonator neck length. - A single resonator (configuration 1) was inserted into the test section at position 2 (see fig. 9(a), p. 12). The chamber was excited by an electrical speaker to the first standing tangential, second standing tangential, and first radial modes to determine the effect of frequency. At each frequency, the resonator cavity volume was tuned to maximum damping and the sound pressure level (SPL) was measured. This procedure was repeated for configurations 2 to 5.

Determination of effect of resonator volume. - A single resonator (configuration 7) was inserted into position 2 with speaker and microphone as indicated in figure 9(a). The cavity was excited to the first standing tangential mode, and the resonator volume was varied incrementally with the chamber SPL recorded at each position.

Determination of effect of wave amplitude variation. - In order to determine the effect of wave amplitude on resonator damping, the bandwidth of the first standing tangential mode was measured for a range of sound levels. This measurement is discussed in the section THEORY. A single resonator (configuration 6) was inserted at position 2 (fig. 9(a)). The resonator volume V was tuned to maximum damping at the 130-decibel level and maintained. The amplitude of the mode was varied from 130 to 155 decibels, and the bandwidth was recorded at each sound level.

Tests With Perforated Liner

In order to determine the effect of a gradual increase in acoustic liner absorption area, a 0.60-inch-thick 5/16-inch-hole-diameter liner was mounted within the closed-end test section. A single speaker was used to drive the first standing tangential mode. A probe-type microphone was inserted into the chamber diametrically opposite the speaker to determine the damping both by decay rate and by the decrease in the SPL.

Initially, all liner holes were masked completely by stiff tape. The longitudinal column of resonators opposite the speaker (the column containing the microphone) was unmasked gradually, one hole at a time, until all resonators in the column were unmasked. The decay rate and SPL of the mode were recorded at every step.

For circumferential unmasking, the procedure also started with a completely masked liner. The circumferential row that contained the speaker and microphone was unmasked gradually, starting from a point opposite the speaker and continuing one hole at a time.

Tests of Other Liner Parameters

For all liner configurations (table II, p. 13) the following procedure was instituted: The liner was mounted firmly within the test section by eight bolts to ensure that mechanical vibrations did not interfere with the results. A probe-type microphone was inserted into the test section by way of a small hole through the chamber wall and the liner. The location of the probe microphone was dependent on the type of test and the mode studied. Initially, a frequency-amplitude plot was obtained; at the resonant frequencies corresponding approximately to the theoretical frequencies of the blank liner system, the spatial pressure distribution was probed. This procedure was necessary to identify

correctly the modal frequencies.

For the steady-state SPL, the probe tube was moved to the appropriate position for the pressure maximum, corresponding to the mode, and the SPL measurement was made. In order to obtain amplitude decay rates, the driver or drivers were turned off, and a trace of the decay was photographed on an oscilloscope screen. For the bandwidth measurement, the frequencies at 3 decibels off the peak were measured on either side of the peak, corresponding to the half-power point.

Mean Flow Variation

The mean flow rate in the tunnel was measured by a Pitot-static probe that could be moved diametrically across the tunnel and longitudinally the length of the test section. Once the steady-state turbulent flow profile was established, the testing procedure became the same as for the closed-end test section.

DATA REDUCTION

Conversion of Decay Rate to k_r

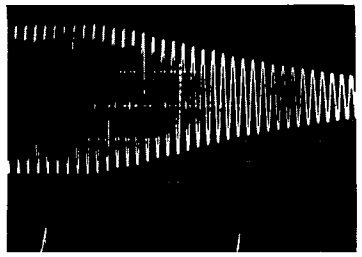

(a) Photographic view.

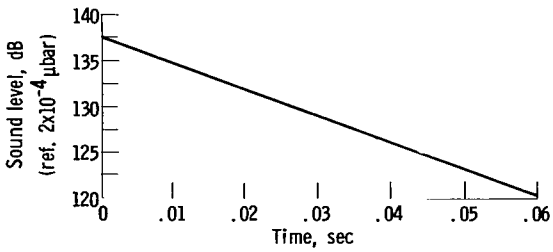

(b) Semilogarithmic plot. Liner parameters: liner thickness, 0.25 inch; hole diameter, 3/8 inch; input wave frequency, 728 hertz; center-to-center spacing of perforations, 1 inch; no flow; electric driver used; slope, 280 decibels per second.

Figure 11. - Decaying sound wave in test section.

Figure 11(a) is a sample data photograph of a decaying acoustic field in the test section. The trace envelope was a smooth exponential curve of pressure against time. Figure 11(b) presents information from figure 11(a) as a semilogarithmic plot of pressure against time. The slope of the line was measured as 280 decibels per second.

From the following equation

$$\mathrm{SPL} = 20 \log_{10} \frac{p}{p_{ref}}$$

the change with respect to time is

$$\frac{d(\mathrm{SPL})}{d\tau} = \frac{8.686}{p} \frac{dp}{d\tau}$$

It has been shown that $p = p_{max}\exp(-k_n\tau)$ for any point in the chamber. Substituting yields

$$k_r = k_n = \frac{1}{8.686}\frac{d(SPL)}{d\tau}$$

Conversion of Reduction in Steady-State Sound Pressure Level to k_p

It has been shown previously that, for the same system with two different damping configurations, the ratio of the k_n's is the inverse ratio of the sound pressures. If the k_n is determined for the blank test chamber by decay-rate measurement and called k_1 and if the pressure level corresponding to k_1 is p_1, then, for the same mode in the test chamber only with a damping device installed, if the pressure level at the same position is p_2,

$$k_p = k_2 = \frac{p_1}{p_2}k_1$$

Error Analysis

In order to determine the error in the data presented, the following table is given:

Type of reading	Error	Nominal value of reading	Relative error, percent
Decay rate	±20 dB/sec	200 sec^{-1}	±10
Sound pressure level (SPL)	0.5 dB	140 dB	1
Frequency	1 Hz	1500 Hz	1
Position of single resonator piston	±0.03 in.	0.5 in.	±6

The decay rates were measured by comparing the envelope of the decaying pressure trace similar to that of figure 11(a) (p. 17) with a series of theoretical curves for exponential decay rates. The theoretical curves cannot be matched closer than ±20 decibels per second to the experimental data. Errors in the measurement of SPL and frequency are due to lack of precision in the instrumentation. The relative errors were computed by dividing the reading error by a nominal value of the reading.

Effect of Humidity

For the present experiment, no effort was made to correct for the effects of gas volume losses within the test section, as was done in reference 7. The volume losses are molecular relaxation phenomena that are affected by the humidity. A more detailed explanation is given in reference 9.

In reference 9 (p. 238), the maximum deviation in decay rate k_r due to humidity is 1.375 decibels per second for a nominal frequency of 1500 hertz and a change from 10 to 60 percent relative humidity. The value of k_r for an unperforated liner with very low damping is 30 decibels per second. The error in measuring k_r is approximately 20 percent or 6 decibels per second, and this value, therefore, exceeds the maximum error (due to humidity) in k_r by a factor of at least 4. Consequently, the effect of humidity was not corrected for in the experiment.

RESULTS AND DISCUSSION

The following experimental results are presented herein: the frequency response of the empty test chamber, cross-section pressure profiles of the acoustic modes, comparison of first standing and spinning tangential modes, comparison of wave shapes from the output of high-frequency transducers attached to a screeching rocket combustor with the wave shapes of modes in the empty test chamber of this investigation, response of the empty test chamber to random-noise input, experiments with single resonators, and experiments with perforated liners.

Bare Chamber Results

Figure 12 (p. 20) is a frequency - amplitude plot for the test section with a solid wall or blank liner and closed ends. The first tangential, second tangential, first radial, and first longitudinal modes can be identified easily by their frequencies, since there are few modes in the lower end of the frequency spectrum. A linear combination of the first tangential and first longitudinal modes is described in appendix C. The first radial mode has a greater amplitude at the centerline of the chamber than is present at the wall. Therefore, to minimize the relative error, all first radial mode amplitudes and decay rates were measured with the microphone probe located at the centerline. The number of modes in the higher frequency ranges is greater than that in the lower frequency ranges, with more combination modes possible at the higher frequencies. This makes the identification of the modes considerably more difficult.

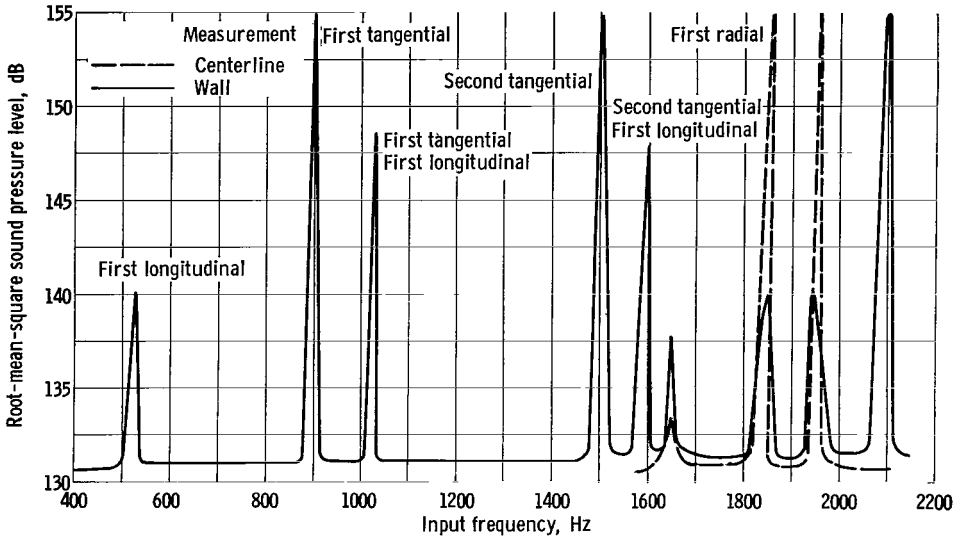

Figure 12. - Frequency response at test section with blank liner and both ends closed.

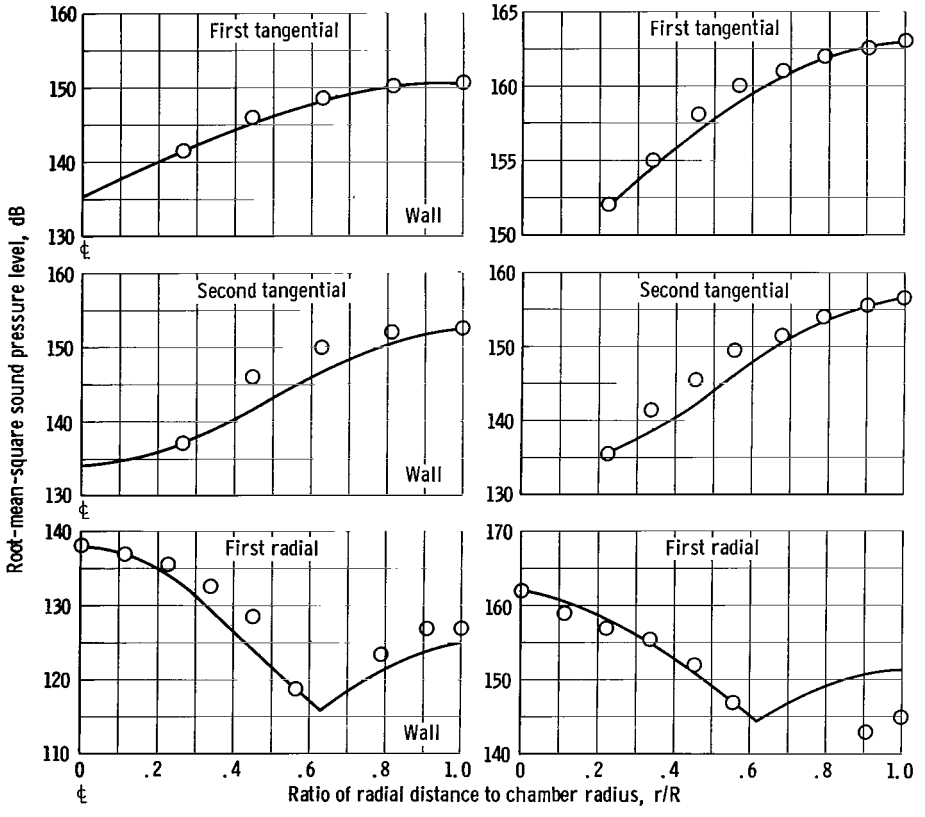

Figure 13. - Sound pressure level as function of radial position for speakers in bare system. Curves, normalized theoretical.

It was necessary to consider the identification of the acoustic modes when a perforated liner was installed in the chamber. For small damping, the modes could have been characterized by their resonant frequencies alone; in many cases, however, the frequency of the mode shifted because of the damping of the liners. In these cases, it was necessary to probe the internal sound field of all the peaks on the frequency spectrum to determine which peak had the cross-section pressure profile corresponding to the mode being investigated (appendix C).

Shown in figure 13 are the cross-section pressure profiles of the first tangential, second tangential, and first radial modes for both the electrical (fig. 13(a)) and electropneumatic drivers (fig. 13(b)). For comparison, a plot of the normalized theoretical pressure profiles with the maximum and minimum values matched to the theoretical curve was included. The comparison between theoretical and experimental profiles indicates that the modes desired can be set up within the test section.

Figure 14 is a comparison of the circumferential profiles of the first tangential

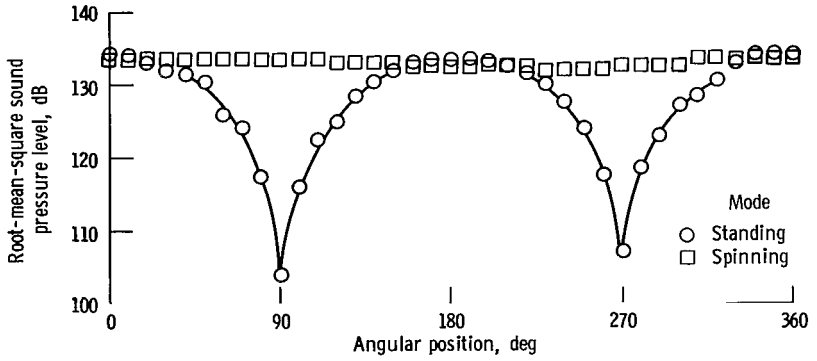

Figure 14. - Circumferential profile of standing and spinning first tangential modes.

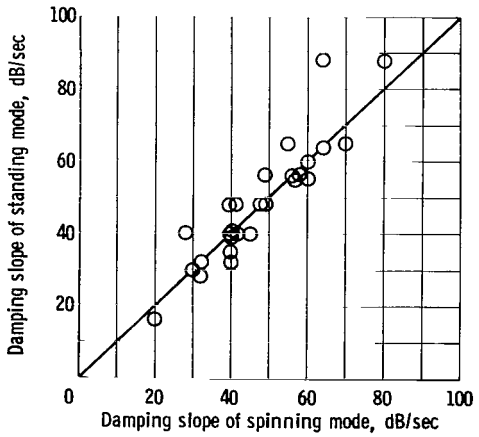

Figure 15. - Comparison of spinning and standing tangential mode decay rates for equivalent configurations.

spinning and standing modes taken with the microphone at the wall of the test section. For the spinning mode, the profile is flat to within experimental error (including the slight difference in output between the two drivers used). The results indicate that both spinning and standing first tangential modes can be established within the test section.

Figure 15 summarizes all damping data taken for both standing and spinning first tangential modes for equivalent damping configurations. The results indicate no difference between the two within experimental error. Accordingly, only the standing first tangential mode results will be presented herein.

Wave Shape Comparison

The use of acoustic waves to study damping devices for combustion stability is questionable unless a similarity between acoustic and screech waves can be shown. An argument for similarity is that, although the internal pressure distribution of a screeching combustor has not been measured, the frequencies of the waves can be calculated by acoustic theory. A counterargument is that screech-wave amplitudes in excess of the mean pressure have been measured, whereas acoustics deals only with waves that are a small fraction of the mean pressure.

As a step toward a resolution of the conflict, the assumption was made that, if the two types of waves had the same transverse spatial or geometric similarity, the distortions of the screech wave could also be seen in acoustic waves.

The results of attempts to match the wave shapes from a screeching rocket combustor and the acoustic test chamber are shown in figure 16. In figure 16(a), the results of exciting a first standing tangential mode within the bare test chamber at the maximum attainable amplitude are presented. The upper trace is the output from a microphone placed at the pressure antinode and shows distortion of the wave caused by the second

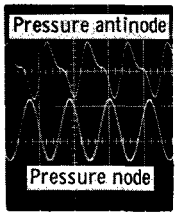

(a) First standing tangential mode in bare test chamber at maximum amplitude.

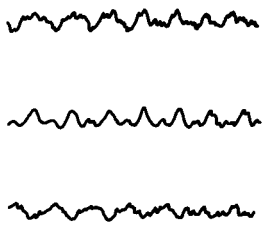

(b) Three high-frequency pressure transducers attached to a screeching combustor.

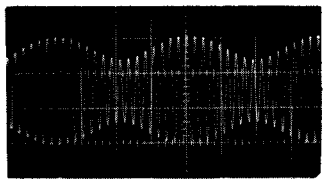

(c) First standing tangential mode and second standing longitudinal mode on two speakers.

(d) High-frequency transducer attached to combustor.

Figure 16. - Comparison of acoustic mode wave shape from bench test section with output of high-frequency pressure transducers on unstable rocket engine.

harmonic. The lower trace is the output of a microphone placed at a pressure node. The small pressure oscillations at the node, when highly amplified, show no distortion.

Presented in figure 16(b) is the output from three high-frequency pressure transducers attached to a screeching combustor. In all three traces and particularly in trace 2, the double-peak characteristic of second harmonic distortion can be seen.

The results of introducing simultaneously a first standing tangential mode with one speaker and a second standing longitudinal mode with a second speaker are presented in figure 16(c). The output trace shown is from a microphone placed at the pressure antinode of the tangential mode. The form of the trace is a modulated sinusoid characteristic of a beating between the two frequencies of the two modes. Figure 16(d) shows the output of a high-frequency transducer attached to a combustor. The wave envelope of figure 16(c) matches closely that of figure 16(d).

The similarity in wave distortions in both acoustic and screech waves indicates that there is a similarity between the two types of waves and lends credence to the use of acoustic waves for evaluating combustion chamber damping systems.

Response of Empty Test Chamber to Random-Noise Input

Presented in figure 17 is a plot of the response of the system to a random-noise input. The principal modes are present and, if the chamber is probed with a microphone and a band-pass filter that is set at a frequency corresponding to a modal peak, the

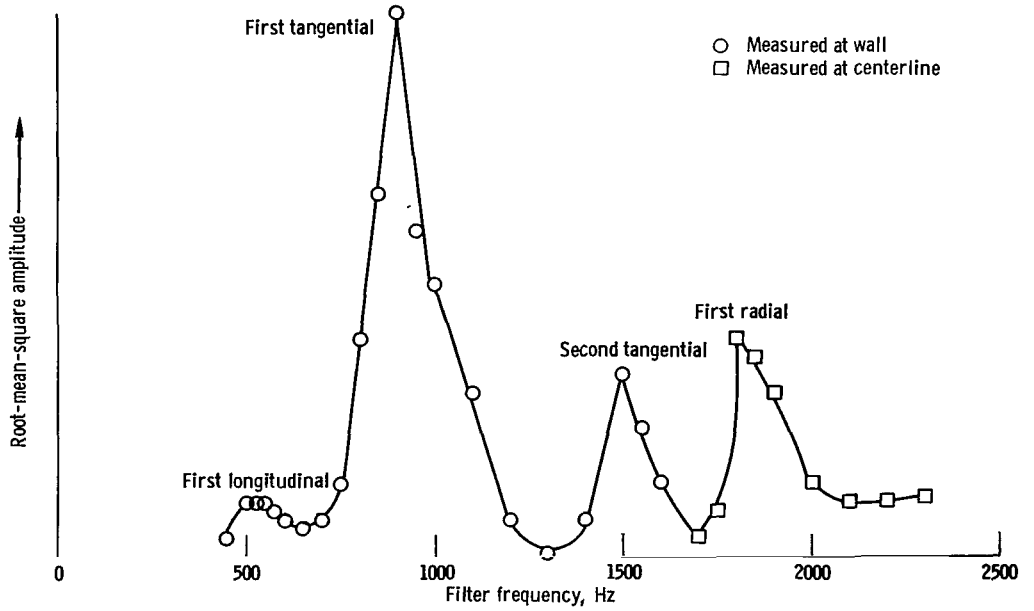

Figure 17. - Frequency response of bare chamber to random-noise input.

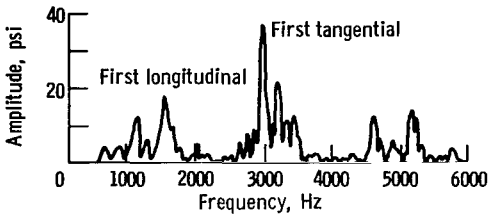

Figure 18. - Amplitude spectral density for hydrogen-oxygen rocket system.

characteristic spatial pressure distribution of the mode is obtained. It may be concluded, therefore, that all the modes are excited simultaneously by the random-noise input and that the amplitude of each mode is the difference between the sound-power input and the damping of the chamber associated with the particular mode. This result indicates that the random noise caused by combustion in an operating rocket engine will distribute itself into the normal modes of the combustion chamber cavity with the proper phase relation and spatial pressure profile of each mode. If the output of high-frequency transducers attached to a rocket engine is analyzed by frequency, a simultaneous series of peaks may be seen, depending on the damping within the combustion chamber. Figure 18 is an example of such an analysis of a hot test (hydrogen-oxygen) of a rocket engine with similar geometric properties to the bare system. The theoretical acoustic modal frequencies for this engine are about 1500 cps for the first longitudinal mode, about 3000 cps for the first transverse mode, and about 5700 cps for the first radial mode.

Single Resonator Results

From preliminary tests of the first liner configurations, it was readily apparent that the liner performance was not completely predictable by theory. Therefore, in order to establish a basis for later comparison with theory, single resonator tests were undertaken.

There were two general types of tests with single resonators, those in which the resonators were mounted on the cylindrical test section (fig. 9(a), p. 12) and those in which the single resonator was attached to a resonance tube (fig. 9(b), p. 12).

Angle-of-incidence apparatus. - The purpose of the angle-of-incidence investigation was to determine the effect of varying the angle between the wave vector and the axis of the resonator neck. Reference 4 indicates the strong effect of angle of incidence on absorption; for an incidence angle of 90°, the absorption is predicted to be zero. For a tangential wave in a cylindrical chamber with a liner, the angle of incidence varies around the circumference of the chamber. At the pressure antinodes, the angle is 0° and, at the nodal points, the angle is 90°. The tangential component of the wave vector is specified by the mode, but the radial component of the wave vector is a function of the absorption of the wall, which is, in turn, a function of the angle of incidence. This difficulty in specifying the angle of incidence leads to the use of the resonance tube for examining angle effects (fig. 9(b)). The wave vector was, for the most part, parallel to the

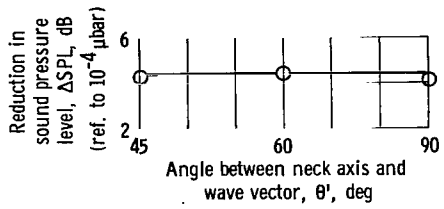

Figure 19. - Amplitude drop with resonator at incidence angles of 45°, 60°, and 90°.

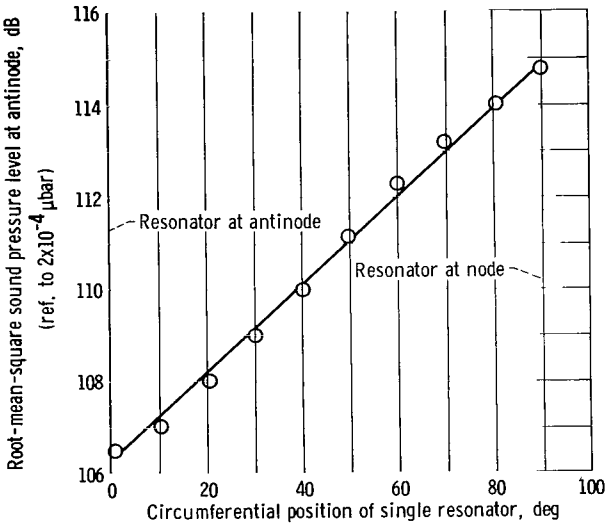

Figure 20. - Effect of variation in angular position of single Helmholtz resonator on sound pressure level in closed-end test section.

walls of the tube at all points along the tube.

The results of the angle-of-incidence investigation are presented in figure 19. The frequency for the first longitudinal mode that placed the resonator neck at a point midway between a pressure node and a pressure antinode was 444 hertz. The tuned resonator volume was the same for the three values of θ'. The results indicate no effect of angle of incidence on absorption, which is a contradiction of the results predicted in reference 4. At present, no explanation is known for the disparity. In accordance with the results, however, there is no apparent advantage in tilting the holes in an acoustic liner to obtain higher absorptions.

Angular position. - Figure 20 shows the variation in sound pressure in the cylindrical test section at a pressure antinode with changes in the angular position of the single resonator. At 90° or $\pi/2$, there is a node for the first tangential standing mode. The resonator produces no damping at this position. As the resonator is moved toward 0°, the sound pressure level in the test section decreases to a minimum, with a maximum reduction of 8 decibels when the resonator is at 0°. The data can be fitted by a straight line to within experimental error. If the linear relation is used, the following expression is derived:

$$p_{max} \propto p_{max}|_{\beta=0}^{\exp \beta}$$

where p_{max} is the pressure maximum at the antinode, $p_{max}|_{\beta=0}$ is the peak pressure at the antinode when the resonator is at an antinode, and β is the angular position of the resonator relative to the pressure antinode. At present, there is no model that can explain this relation; however, maximum damping occurred with the resonator at the pressure antinode.

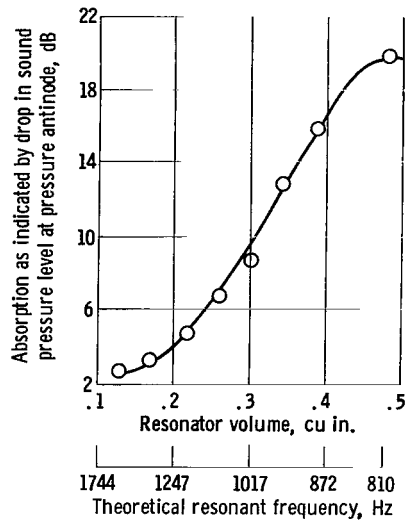

Figure 21. - Effect of resonator volume on absorption of single Helmholtz resonator. Neck length, 13/32 inch; neck diameter, 7/32 inch; mode, first tangential; input wave frequency, 846 hertz; resonator position, at pressure antinode.

Resonator cavity volume. - Figure 21 shows the variation in resonator damping with change in the resonator cavity volume. According to references 3 and 4, the absorption should be a maximum when the resonator is tuned to the wave frequency. Therefore, the data representing the drop in steady-state sound pressure level at a pressure antinode should reach a maximum when the resonator is tuned to 846 hertz. There is a maximum shown in the data, but the calculated resonant frequency corresponding to the point is 810 hertz. This discrepancy in frequency is attributed to errors in measuring the cavity volume used in calculating the resonant frequency (see section Error Analysis) and uncertainty in determining the volume corresponding to perfect tuning. The results, however, show that the equation for calculating the resonant frequency is valid to within experimental error and that the absorption is a strong function of how closely the resonator is tuned to the wave frequency.

Neck length effect on neck correction factor. - A plot of the difference between effective and actual neck length as a function of actual neck length is presented in figure 22. The equation used to calculate ℓ_{eff} from the resonator dimensions and the input frequency is as follows (ref. 3, p. 1039):

$$\ell_{eff} = \frac{A}{V}\left(\frac{c}{2\pi f_0}\right)^2$$

The frequency f was obtained by matching the input frequency with the resonator frequency for maximum damping so that $f = f_0$. If all the other parameters were known, ℓ_{eff} could be calculated. For the theoretical ℓ_{eff}, the equation used was (ref. 4)

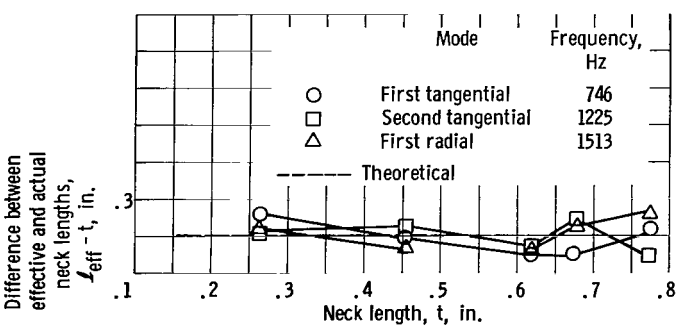

Figure 22. - Effect of neck length on effective length correction factor for single Helmholtz resonators.

$$\ell_{eff} = t + 0.85d\left(1 - 0.7\sqrt{\sigma}\right)$$

The t in this case is neck length whereas, in acoustic liner applications, it would be liner thickness. The theoretical and experimental results are generally in agreement to within experimental error and

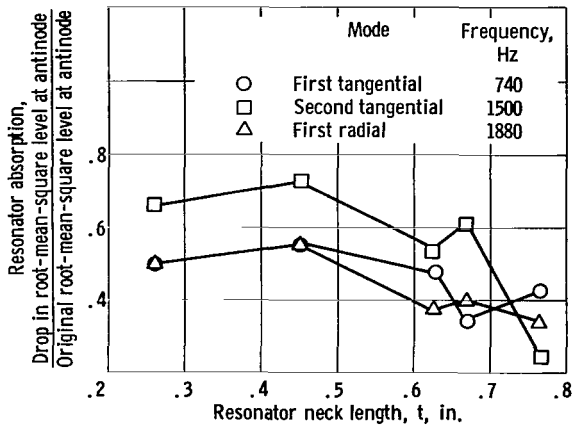

Figure 23. - Effect of resonator neck length on its damping.

show no significant variation with actual neck length.

Liner thickness. - Figure 23 shows resonator damping as a function of neck length. In this figure, the damping values for the first tangential mode are a maximum at a neck length of 0.45 inch and a minimum at 0.67 inch, whereas the second tangential and first radial results each have two damping maxima, one at 0.45 inch and a smaller one at 0.67 inch.

The resonators were tuned to the input wave frequency so that the reactance term X was zero (THEORY section). Therefore, the resonator absorption was caused by only the real part of the impedance θ (eq. (B8)). The equation for the real part of the impedance θ (eq. (B6)) has within it the expression $\epsilon + t/d$. From the THEORY section, it is known that ϵ is a function of the ratio of particle displacement to thickness s/t. However, s is also a function of t (ref. 4), and t/d contains t; hence, the number of maximums and minimums observed and the strong dependence of absorption on liner thickness are possibly caused by the complex relation between t and θ.

Wave amplitude. - The effect of amplitude on absorption is presented in figure 24, where the frequency bandwidth of the modal peak is plotted as a function of the wave amplitude. It has already been stated that $2\pi|\Delta f| = k_n$ (THEORY section). Since k_n is proportional to the resonator damping, figure 24 is actually resonator damping plotted as a function of amplitude. The results indicate an absorption maximum at 140 decibels.

It may be recalled from the procedure for this particular experiment that the resonator was tuned to the input frequency of sound wave. Appendix B (eq. (B7)) shows that, if the resonant frequency f_0 is equal to the input frequency f, the term X is zero. Consequently, the absorption α is a function of the liner acoustic resistance θ only, and any change in absorption must be caused by a change in θ. It can be seen (eq. (B6) and the discussion following it) that the nonlinear correction factor ϵ is increased by increasing the amplitude, while all other terms in the equation for θ remain the same. A monotonic increase in ϵ, therefore, caused θ to increase. Since the

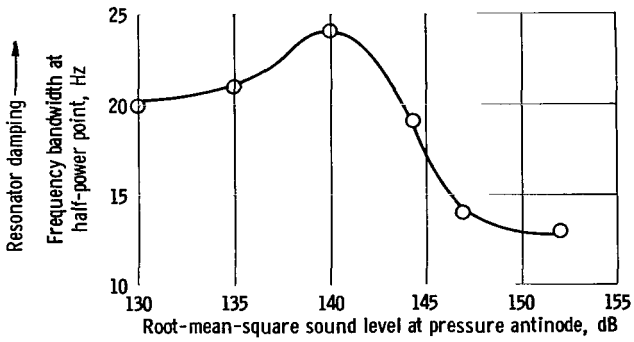

Figure 24. - Effect of variation in sound level on damping of single Helmholtz resonator in closed-end test section.

absorption rose to a maximum and then decreased, θ was originally less than 1, and further increases in ϵ cause θ to increase to 1 and then to exceed 1, which results in a maximum in α (eq. (B8)). Thus, resonator absorption is a strong function of wave amplitude, and the complex relation between the two can be explained by the theoretical equations.

Perforated Liner Results

All the data are presented in the form of the damping coefficients k_r and k_p (see DATA REDUCTION section). The experimental damping coefficients are compared with the theoretical absorption coefficients for acoustic liners. The equations for calculating α are given in the THEORY section. The numerical values of α cannot be converted into damping coefficients because of the distortion of the pure acoustic wave field by the damping on the walls. (Further explanation of this problem can be found in ref. 10, ch. 8, pp. 410-412.)

For any problem, however, the trends of theoretical and experimental results should be the same, with an increase in α causing an increase in the damping coefficients. In all cases, both k_p and k_r are presented. No method exists at this time to determine which of the two is more valid.

Frequency shift. - Figure 25 shows the changes in modal frequency and amplitude that occur when a perforated liner is tested. Only the peaks for the first tangential, second tangential, and first radial modes are displayed for the sake of clarity. For the liner parameters indicated in figure 25, the calculated resonant frequency of the liner is 1051 hertz, and it was found that the liner shifts chamber resonant frequency in either direction away from the resonant frequency as well as decreasing the amplitude within the chamber. The frequency shift is caused by the imaginary part of wall impedance X, differing from zero either positively or negatively. A more complete discussion is given in appendix D.

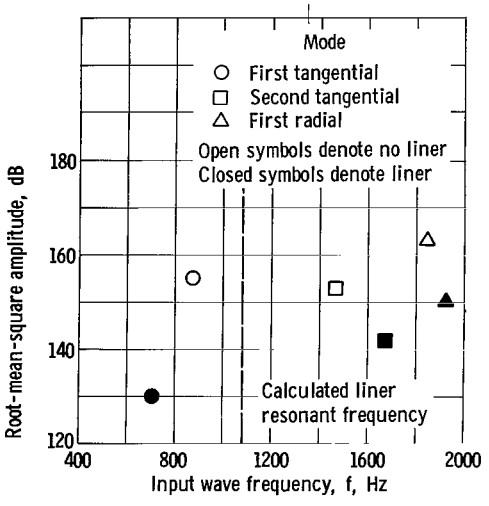

Figure 25. - Frequency shift and amplitude decrease for liner in closed-end test section. Liner thickness, 0.60 inch; perforation, 5/16 inch; open area, 10 percent; complete partitions; liner resonant frequency, 1051 hertz.

Number of resonators. - Axial unmasking gives an almost linear increase in damping with the number of resonator necks uncovered (fig. 26(a)). This increase is caused by the uniform axial distribution of the tangential modes in the test chamber. Therefore, all axial positions

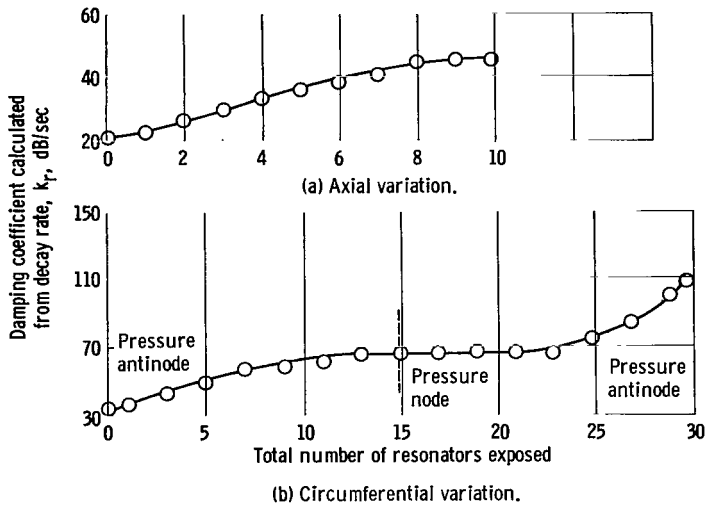

Figure 26. - Effect of variation in maximum number of resonators on damping in closed-end test section.

are equally favorable for damping devices. This would not be true for a rocket combustor with a localized region of high-pressure oscillations, where some axial positions would be more important than others.

The results of the circumferential unmasking are shown in figure 26(b). Unmasking was initiated in the region of a pressure antinode, and the change in damping with number of uncovered holes (slope of the line) was initially steep. Holes 10 to 20 are in the region of the pressure node and, therefore, no large increase is noted with each hole opened, while holes 20 to 30 are in the region of the other antinode and the slope of the line is again steep. The results verify that resonators are effective only at or near pressure antinodes, the same result as was obtained with a single resonator in figure 20 (p. 25).

Partitioning liner-back cavity. - The effect of the variation in the partitioning behind a liner is presented in figure 27 (p. 30). The results are given for two different modes, first radial and first tangential. The purpose of the partitions is to isolate the cavity behind each hole in a liner to prevent a tangential wave from inducing a circumferential particle motion behind the liner. The present design theory does not take partitions into account.

The criterion for a cavity to be a Helmholtz resonator is that its largest dimensions be very small compared with the wavelength of the oscillation it is to absorb. If a tangential induced gas motion occurs behind the liner, this criterion is no longer satisfied; consequently, the liner would no longer be a true Helmholtz resonator array and might not absorb as well. The radial mode has no tangential components and, therefore, would not be expected to induce any tangential motion behind the liner.

The data presented confirm the induced tangential motion with the longitudinal partitions having an effect on the tangential mode damping and no effect on the radial mode

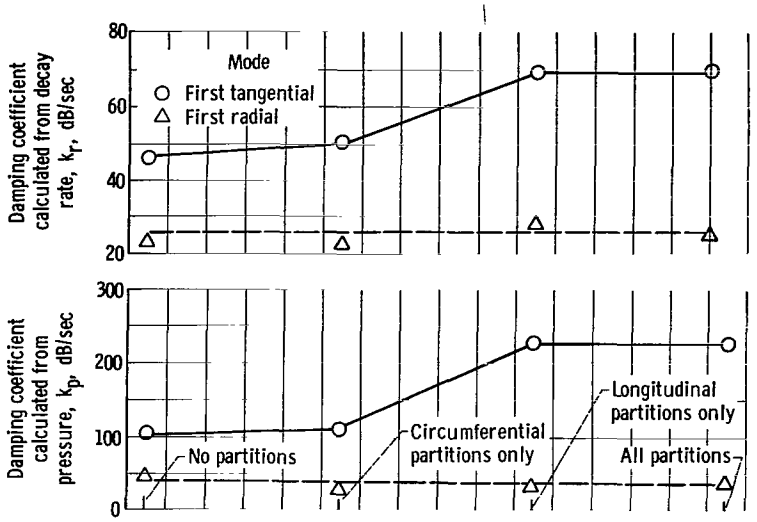

Figure 27. - Comparison of damping coefficients based on both pressure and decay rate for first tangential and first radial modes of oscillation with various conditions of backing cavity isolation. Electrical drivers; liner thickness, 0.45 inch; hole diameter, 5/16 inch; flow velocity, 0; hole spacing, 1 inch; backing distance, 0.55 inch.

damping. The longitudinal baffles would prevent any overall motion in a tangential direction behind the liner, whereas the circumferential baffles contribute nothing to blocking a tangential motion and, therefore, have no effect on damping.

Liner thickness. - The data in figure 28 show the effect of liner thickness on absorption. In figure 28(a), the theoretical α peaks at a thickness of 0.4 inch for the first tangential mode and decreases for the first radial mode with increasing liner thickness.

In figure 28(a), the shaded symbols, which correspond to the completely partitioned liners, show agreement in the curve shape between k_r, k_p, and α. For all three, the absorption for the first tangential mode decreases as the thickness of the liner is increased above 0.4 inch, and the absorption for the first radial mode decreases over the entire range of liner thicknesses shown. The unpartitioned data for the first radial mode compare well with the partitioned results. This was to be expected, based on the results of figure 27, where partitions had no effect on radial modes. The unpartitioned results for the first tangential mode, however, do not compare with the partitioned results or with α. The significant effect of partitions on absorption can be noted.

Another feature of figure 28(a) that should be noted is the reasonably good comparison in curve shapes between the theoretical and experimental data coupled with the low values of theoretical absorption ($\alpha < 0.1$). Reference 10 (p. 402) indicates that low absorption does not seriously distort the acoustic field of the mode, and the relation between the k's (k_p and k_r) and α remains simple.

The results for the second tangential mode, presented in figure 28(b), indicate that the effect of the partitions was to lower significantly both the theoretical and experimental

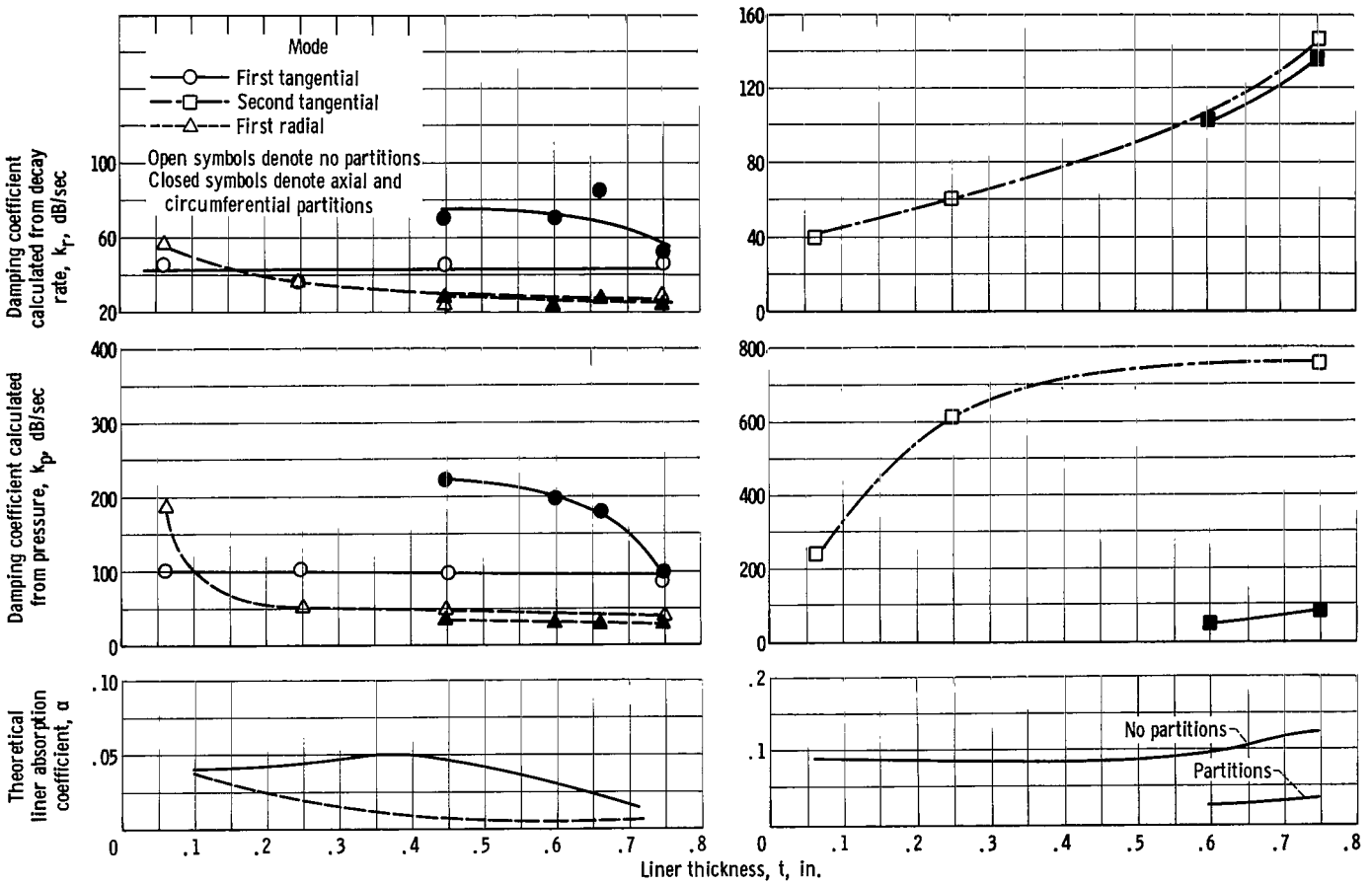

(a) First tangential and first radial modes.

(b) Second tangential mode.

Figure 28. - Comparison of damping coefficients based on both pressure and decay rate and theoretical absorption coefficient as functions of liner thickness for first tangential and first radial modes of oscillation. Perforation, 5/16 inch; mean flow velocity past liner, 0; hole spacing, 1 inch; back distance neck length, 1 inch.

liner absorptions. This negative effect was caused by the volume of the partitioning material, which was sufficient to detune the resonant cavities of the partitioned liner by decreasing the volume V. The effect of detuning the cavity by a slight amount was apparently much more significant for the second tangential mode than for the first tangential mode.

The effect of increasing liner thickness (fig. 28(b)) is to increase liner absorption for the second tangential mode. The shapes of the theoretical and experimental curves are not comparable, however, and this fact, coupled with the high theoretical absorptions ($\alpha > 0.1$), indicates that the acoustic field may have been seriously distorted by the absorption.

The shape of the curves in figure 28 is primarily due to the variation in the liner resonant frequency as the thickness is varied (eqs. (2) and (3)). This effect differs from the single resonator result of figure 23 (p. 27), since no effort was made to retune the liner at the different thicknesses. In general, the theoretical absorption α can be used to predict the effect of liner thickness absorption.

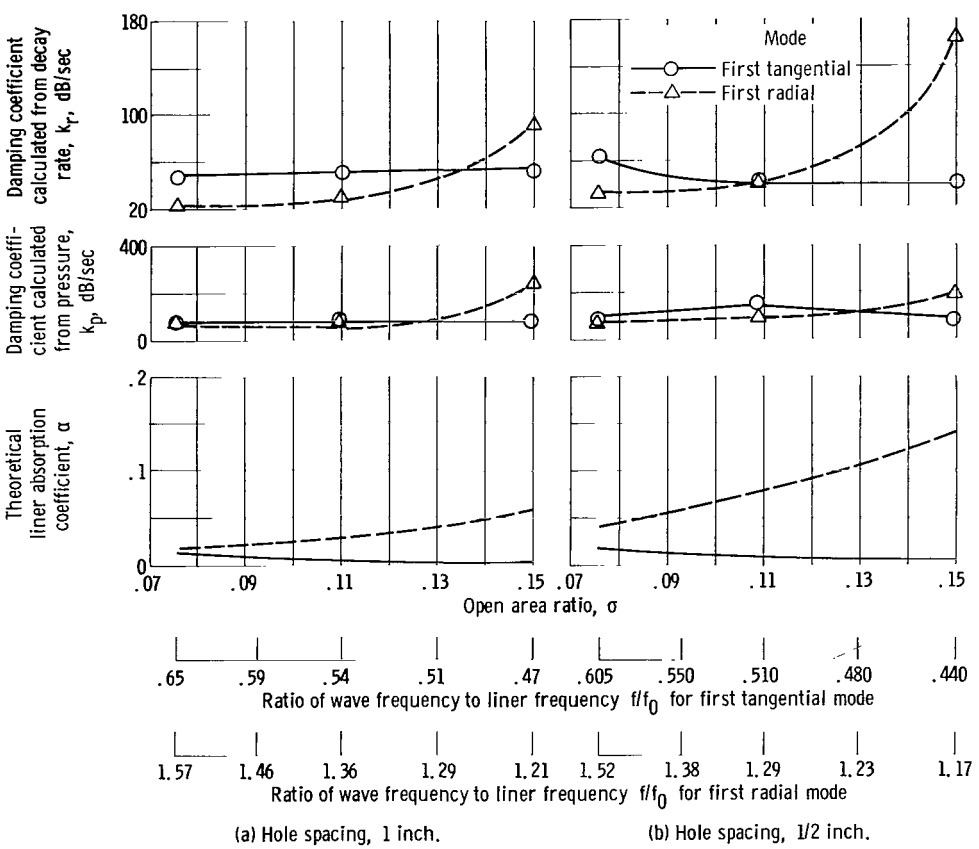

(a) Hole spacing, 1 inch. (b) Hole spacing, 1/2 inch.

Figure 29. - Comparison of damping coefficients based on both pressure and decay rate and theoretical absorption coefficient as functions of open area ratio and ratio of wave frequency to liner frequency for first tangential and first radial modes of oscillation. Liner thickness, 0.75 inch; back distance, 0.25 inch; no partitions.

Open area ratio and hole diameter. - Figure 29 shows the effects of open area ratio σ on liner absorption. The results of figure 29(a) are for a hole spacing of 1/2 inch on a square array, while the results of figure 29(b) represent hole spacings of 1 inch. Both indicate the strong effect of σ on liner absorption.

The variation in open area ratio is equivalent to a variation in liner resonant frequency or, with constant wave frequency, to a variation in the ratio of wave frequency to liner frequency f/f_0. Equations (5) and (7) show that, as f/f_0 approaches unity, the absorption α rises to a maximum. The data presented in figure 29 show the same trend, with absorption increasing as f/f_0 approaches unity. Thus, the principal effect of variations in open area ratio is the variation of the tuning of a liner.

Differences between figures 29(a) and (b) are caused by the differences in hole spacings. Equation (1) shows that differences in hole spacings for the same open area can be obtained only by varying the hole diameter. Theoretical differences between the two configurations are, therefore, caused by expressions where the hole diameter d appears independently of the open area σ. Equations (2) and (6) are two such expressions. They determine ℓ_{eff} and θ, respectively, and cause α to be a function of d independent of σ. As an example of the preceding argument, the maximum theoretical absorption for the first radial mode in figure 29(a) is one-half of the maximum in figure 29(b). The same result is seen in the maximum value of k_r.

Based on the theoretical and experimental results of figure 29, the theoretical equations apparently can predict qualitatively not only the effect of open area ratio σ on absorption but also the effect of d independent of σ.

Backing distance. - The data displayed in figure 30 (p. 34) were obtained by varying the liner-back distance from 0.16 to 0.75 inch for a 1/4-inch-thick liner with 5/16-inch-diameter holes on a 1-inch-square array. According to equation (3), a variation in liner backing distance $e\ell$ is equivalent to a variation in liner resonant frequency f_0. In addition, as the ratio of wave to liner frequency f/f_0 approaches unity, the absorption rises to a maximum. Consequently, a more meaningful scale than liner-back distance would be f/f_0. Both the theoretical and experimental curves presented in figure 30 indicate maximum values in damping as f/f_0 approaches unity. The value of f/f_0 at which the experimental damping coefficients reach a maximum was not determined, but it is apparently greater than unity.

A possible explanation lies in the manner in which the liner-back distances were varied. As noted herein, a series of concentric metal cylinders was fitted around the outside of a liner, but within the test section, to vary the back space without varying the liner thickness. These shells may have shifted and could have altered the backing distance by a sufficient margin to cause the discrepancy between theoretical and experimental results. The results, however, indicate that the effect of tuning and detuning the liner by changing the backing distance can be predicted by the design equations.

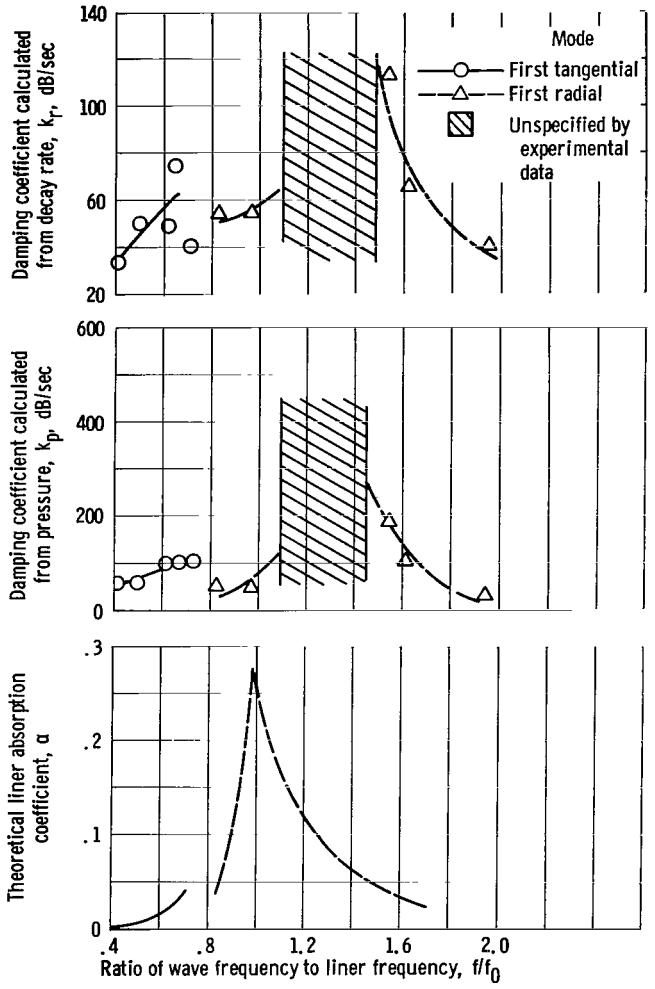

Figure 30. - Comparison of damping coefficients based on both pressure and decay rate and theoretical absorption coefficient as functions of ratio of wave frequency to liner frequency for first tangential and first radial modes of oscillation. Perforation, approximately 5/16 inch; liner thickness, 1/4 inch; hole spacing, 1 inch; no partitions.

Effect of two hole diameters on liner damping. - A major problem in the use of perforated acoustic liners is the narrow frequency range over which the liner can effectively absorb energy. One possible method for expanding the energy absorption bandwidth is to have more than one hole size on any one liner (ref. 11). Figure 31 presents data from a liner with alternating 5/16- and 3/8-inch-diameter holes. There is good agreement between experimental and theoretical results, with the double hole size liner lying midway between a liner with all 5/16-inch holes and a liner with all 3/8-inch holes.

This result indicates that a liner formed by superimposing two different hole diameters behaves as an average of two different liners, each with only one hole diameter.

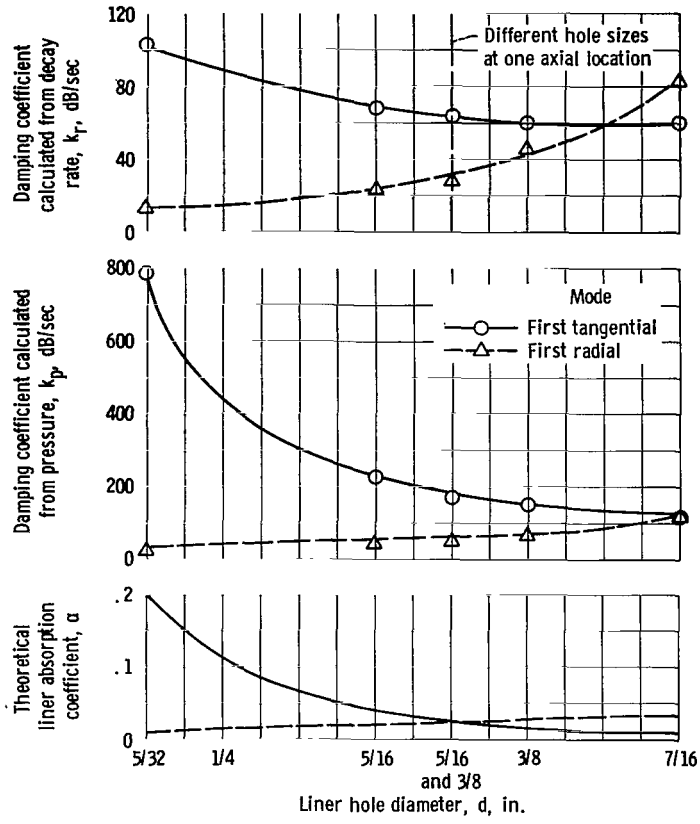

Figure 31. - Comparison of damping coefficients based on both pressure and decay rate and theoretical absorption coefficient as functions of hole diameter for first tangential and first radial modes of oscillation. Effect of two hole sizes (5/16-in. diam and 3/8-in. diam, spaced 1 in. apart) on one liner is shown. Liner thickness, 0.45 inch; back distance, 0.55 inch; hole spacing, 1 inch; mean flow velocity past liner, 0; circumferential and longitudinal partitions.

Although the size of the absorption bandwidth (the frequency range over which α is over one-half its maximum value) has not been measured, reference 11 indicates that it will encompass the bandwidths of the two liners, one with all 3/8-inch hole diameters and the other with all 5/16-inch hole diameters. The center of the expanded bandwidth will be the arithmetic average of the two single-hole-size liners, just as was found experimentally. Thus, it seems reasonable to conclude that the bandwidth has been expanded. The ability to expand the bandwidth of the liner by providing it with a range of hole sizes indicates that a liner may be designed to operate effectively over a wide range of frequencies. More experimental work is required to verify the broadened bandwidth.

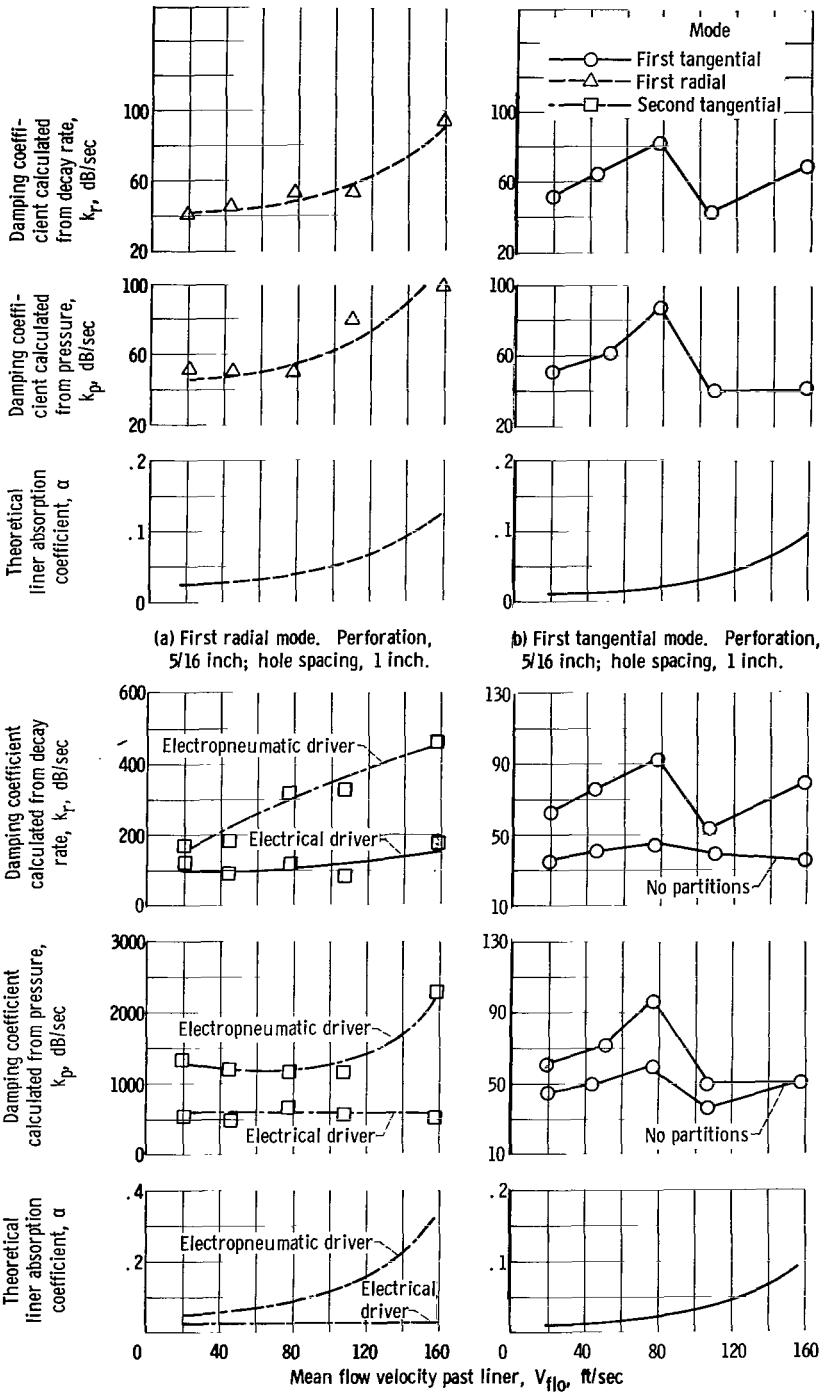

(a) First radial mode. Perforation, 5/16 inch; hole spacing, 1 inch.

(b) First tangential mode. Perforation, 5/16 inch; hole spacing, 1 inch.

(c) Second tangential mode. Perforation, 5/16 and 3/8 inch; two drivers used to obtain differences in wave amplitude.

(d) First tangential mode. Perforation, 5/16 inch.

Figure 32. - Comparison of damping coefficients based on both pressure and decay rate and theoretical absorption coefficient as functions of mean flow velocity past liner for first tangential, second tangential, and first radial modes of oscillation. Liner thickness, 0.45 inch; back distance, 0.55 inch; partitions, circumferential and longitudinal.

Mean flow past liner. - Figures 32(a) and (b) show the effect of flow past a liner on its absorption. The liner used for this test was 0.45-inch thick and had 5/16-inch hole diameters on a 1-inch spacing and both circumferential and longitudinal partitions in the backing cavity. Figure 32(a) shows the results for the first radial mode. The theoretically predicted α gradually increases as the flow past the liner is increased to 159 feet per second. The experimental damping coefficients show good comparison with one another and with the theory, which indicates the validity of the expressions from reference 5 for predicting the effect of mean flow.

Figure 32(b) shows the results for the first tangential mode. The theoretical curve is similar to that of figure 32(a), but the experimental data have a markedly different trend. The occurrence of a peak in absorption at 80-feet-per-second flow velocity cannot be accounted for by the present set of design equations. Reference 5 (vol. III, p. 6), however, indicates that there may be an interaction between the flow field and the acoustic field when the ratio of the flow past the liner to the actual hole spacing approximates the sound frequency (i.e., $V_{flo}/a = f$). With the 1-inch hole spacing and a V_{flo} of 80 feet per second, the flow-spacing ratio gives a frequency of 960 hertz, while the input frequency, which varied because of frequency shift considerations, was approximately 900 hertz. If it is remembered that the velocity past the liner in the immediate vicinity of the holes is not known exactly, the two frequencies can be considered close enough to satisfy the interaction criterion.

The empirical flow correlations of reference 5, which have been incorporated into the theoretical equations, were based on experiments that did not involve standing acoustic waves, but rather traveling longitudinal waves, which may account for the inadequacy of the theoretical-design equations to explain the observed results.

For a rocket combustor with a gas velocity of 1600 feet per second past the liner and a 1-inch axial hole spacing, the pseudofrequency obtained by dividing flow by spacing is approximately 20 000 hertz, which is probably an order of magnitude higher than the screech frequencies commonly observed (ref. 1). Since this is true, the present equations for the effect of flow should be adequate for design purposes for every engine with high axial gas velocities. However, should the flow velocities be significantly lower in a system where a liner is to be used, there may be some advantage to designing for a flow-spacing interaction.

Mean flow and high wave amplitude. - In order to determine if the combined effects of flow past a liner and high-amplitude acoustic oscillations could have unforeseen effects on liner absorption, a liner was tested at the maximum sound level of both the electric and the electropneumatic driver units over a range of flows past the liner. The liner tested was 0.45-inch thick with 5/16-inch and 3/8-inch holes, alternately spaced 1-inch apart, and both circumferential and longitudinal partitions in the backing cavity. The second tangential mode was used, since this mode showed no flow-wave interaction.

The sound level created with the electropneumatic drivers with the liners was approximately 160 decibels, and the sound level created by electric drivers with the liner was 20 decibels lower. The results are shown in figure 32(c).

The curves for the theoretical values of α indicate that the increased sound level caused by the electropneumatic drivers raises the absorption to a considerably higher level. The experimental data compare with one another insofar as the shape of the curves, which lends credence to the theoretical equations that predict the effects of high amplitude and flow on absorption. The results indicate that the combination of high sound level and flow past the liner does not appear to have any unforeseen effects.

The aforementioned results have shown the effects of flow on partitioned liners, but no comparison has been made between partitioned and nonpartitioned liners over the flow range used. Figure 32(d) shows the results of such a test. The liner used had a thickness of 0.45 inch and a hole diameter of 5/16 inch. The first standing tangential mode was used.

The experimental results for the partitioned liner are the same as those of figure 32(b). A comparison of the data for partitioned and unpartitioned liners indicates that the effect of partitions is to increase damping over the flow range tested and that the flow-acoustic interaction previously measured also occurs with unpartitioned liners.

SUMMARY OF RESULTS

The following results were obtained from experiments on the mechanical absorption of acoustic oscillations in a simulated rocket combustion chamber:

1. There is no apparent difference in the absorption of spinning and standing tangential waves by an acoustic liner.

2. The similarities in wave distortions between acoustic and screech waves indicates that there is a dynamic similarity between the two types of waves. This similarity lends credence to the use of acoustic waves for evaluating combustion chamber damping systems.

3. If the combustion system in a rocket engine is a source of random noise, the output of high-frequency transducers attached to the rocket should be a simultaneous set of the modal peaks.

4. There is no advantage to tilting the holes of an acoustic liner to increase absorption.

5. Maximum absorption is obtained when a resonator is placed at a pressure maximum.

6. The absorption of a resonator is a strong function of how closely it is tuned to the wave frequency. Maximum absorption is obtained when the resonator frequency is equal to the wave frequency.

7. The effect of thickness on resonant absorption, excluding tuning effects, is strong and is complicated by nonlinear wave amplitude effects.

8. The effect of wave amplitude on resonant absorption can be explained by the theoretical expressions.

9. A liner that is not tuned exactly to the wave frequency tends to shift the modal frequencies in either direction away from the liner resonant frequency.

10. In this investigation, all axial positions in the chamber were equally favorable for damping devices. This would not be true for a rocket combustor with a localized region of high pressure oscillations.

11. Longitudinal partitions in the back cavity aid in damping tangential waves.

12. The comparison between theoretical liner absorption coefficients and experimental damping coefficients became poorer when the liner absorption coefficient was greater than 0.1.

13. Results indicate that a liner formed by superimposing two different hole diameters behaves as an average of two different liners, each with only one of the hole diameters. The absorption bandwidth, however, may be greatly expanded. Consequently, by proper choice of a range of hole sizes, a perforated liner may be designed to operate effectively over a wide range of conditions.

14. When there is no frequency - hole spacing - flow interaction, the theoretical expressions for the effect of flow apparently predict the experimental trends.

15. The effect of partitions is consistent over the range of flows tested.

16. The expression for calculating the effective length of a resonator neck is valid to within experimental error.

Lewis Research Center,
National Aeronautics and Space Administration,
Cleveland, Ohio, July 27, 1966,
128-31-06-05-22.

APPENDIX A

SYMBOLS

A	area of perforation
a	center-to-center spacing of perforations
c	sonic velocity
D	chamber diameter
d	perforation or hole diameter
$e\ell$	liner-back space or gap height
f	input wave frequency, Hz
f_0	absorber resonant frequency
Δf	bandwidth
i	$\sqrt{-1}$
J_n	Bessel function of first kind of order n
$\overline{K}$	acoustic source strength
k_n	damping coefficient of n^{th} mode
k_p	damping coefficient calculated from reduction in steady-state sound pressure level
k_r	damping coefficient calculated from slope of wave decay rate
ℓ	chamber length
ℓ_{eff}	effective length of resonator neck or effective liner thickness
m,n	integers
$\Delta n\ell/d$	nonlinear correction factor
p	pressure
p_{max}	pressure maximum with position or time in test chamber
p_{ref}	reference pressure, 2×10^{-4} μbar
R	chamber radius
r	radial distance
$\overline{S}_I$	surface integral of ψ^2 and γ
SPL	sound pressure level, dB
s	acoustic particle displacement
t	liner thickness or resonator neck length
V	volume of resonant cavity per perforation
V_{flo}	mean flow velocity past liner
$\overline{V}_I$	volume integral of ψ^2
X	imaginary part of liner impedance
Y	liner admittance
Z	liner impedance
z	axial distance
α	liner absorption coefficient
β	angular position of resonator relative to driver position
γ	imaginary part of liner admittance
ϵ	nonlinear correction factor

ζ	angular position
η	real part of liner admittance
θ	real part of liner impedance or acoustic resistance
θ'	angle of incidence between wave vector and axis of resonator neck
μ	shear viscosity of gas in resonator neck
ρ	density of gas in resonator neck
σ	liner area ratio or open area ratio
τ	time
ψ	acoustic potential
ω	angular frequency
ω_n	angular frequency of n^{th} mode shifted
ω_{on}	angular frequency of n^{th} mode unshifted
ω_r	angular frequency based on wall boundary condition
ω_z	angular frequency based on end boundary condition
ω_1, ω_2	angular frequencies corresponding to half-power point on frequency response curve

APPENDIX B

ACOUSTIC LINER THEORY

An acoustic liner may be viewed as a number of enclosed cavities, each with a narrow opening or neck. The response of the cavity and neck to an acoustic wave can be analyzed by treating the volume of the cavity as a capacitance caused by the compressibility of the gas contained and treating the gas within the neck and its immediate region as an inductance and a resistance. This lumped-parameter approach (ref. 10, p. 235) provides an expression for the resonance frequency of the cavity.

$$f_0 = \frac{c}{2\pi}\sqrt{\frac{A}{\ell_{eff}V}} \tag{B1}$$

Oscillatory gas motion occurs not only within the resonator neck but in the immediate vicinity of the neck, so that ℓ_{eff} is the sum of the neck length plus some correction factor for the extra resonating mass.

The ratio of the perforation area A to the volume per perforation V is also equal to the ratio of the perforation area per unit cross-sectional area of the resonator cavity to the volume per unit cross-sectional area of the resonant cavity:

$$\frac{A}{V} = \frac{\sigma}{e\ell} \tag{B2}$$

Hence, the resonant frequency of a liner can be expressed as

$$f_0 = \frac{c}{2\pi}\sqrt{\frac{\sigma}{e\ell\left(\ell_{eff}\right)}} \tag{B3}$$

If the perforations on the surface of the liner are relatively near one another (ref. 4), the liner may be treated as a uniform impedance Z. This impedance is the sum of a real part θ and an imaginary part X, so that

$$Z = \theta - iX \tag{B4}$$

The expression for the ratio of absorbed to incident acoustic intensity is taken from unpublished data of G. E. Canuel (Pratt and Whitney Aircraft):

$$\alpha = \frac{4\theta}{(\theta + 1)^2 + X^2} \tag{B5}$$

The α indicates how efficient a liner is in absorbing the acoustic energy incident on it. It has a maximum of 1.

An expression for θ, taken from reference 4, is

$$\theta = \frac{4(\pi \mu \rho f)^{1/2}}{\sigma \rho c} \left(\epsilon + \frac{t}{d} \right) \tag{B6}$$

This term is dimensionless and can take on any positive value. The nonlinear correction factor ϵ is of major importance, since it can be at least an order of magnitude greater than t/d. The nonlinear correction factor ϵ is a monotonic function of the amplitude of the incident acoustic wave. The wave, if above an amplitude of 120 decibels, will induce a mean flow or streaming in the neck of the resonator. This streaming increases the acoustic resistance of the neck and gives rise to the ϵ. This nonlinear correction factor ϵ has been defined as $1 + (\Delta n \ell / d)$, and $(\Delta n \ell / d)$ has been correlated with wave amplitude and with the ratio of acoustic particle displacement to liner thickness s/t (refs. 3 and 4 and unpublished data from G. E. Canuel). The term s is directly proportional to the amplitude of the incident wave.

An expression for X is found in reference 4:

$$X = \frac{2\pi f_0 \ell_{eff}}{c \sigma \theta} \left(\frac{f}{f_0} - \frac{f_0}{f} \right) \tag{B7}$$

If $f = f_0$, the resonator is then tuned to the input wave frequency, and $X = 0$. If this occurs, equation (B5) for α reduces to

$$\alpha = \frac{4\theta}{(\theta + 1)^2} \tag{B8}$$

If $\theta = 1$, then $\alpha = 1$. The objective in designing a liner is to tune the device to the frequency of the wave that is to be absorbed, so that $X = 0$, and then to adjust θ as close as is possible to 1 to maximize α.

The effect of mean flow past the resonator neck is twofold: the turbulence at the liner surface due to the flow reduces ℓ_{eff} by an erosive process and causes a subsequent rise in f_0, and, the turbulence penetrates into the resonator neck and increases the acoustic resistance θ in a manner similar to the effect of streaming (ref. 12). Correlations for the shift in f_0 and the increase in θ are found in reference 5.

APPENDIX C

ACOUSTIC MODES

The fundamental equation for acoustic modes in a cylindrical cavity is

$$\frac{p}{p_{max}} = \cos n\zeta \cos \frac{\omega_z Z}{c} J_n\left(\frac{\omega_r r}{c}\right) \cos \omega\tau$$

$$\omega = \left(\omega_z^2 + \omega_r^2\right)^{1/2}$$

$$\omega = 2\pi f$$

If there are no longitudinal components in the waves, the following modes can be developed:

First standing tangential mode (n = 1):

$$\frac{p}{p_{max}} = \cos \zeta J_1\left(\frac{\omega_r r}{c}\right) \cos \omega\tau$$

$$\omega = \omega_r = 2\pi 0.5861 \frac{c}{D}$$

Second standing tangential mode (n = 2):

$$\frac{p}{p_{max}} = \cos 2\zeta J_2\left(\frac{\omega_r r}{c}\right) \cos \omega\tau$$

$$\omega = \omega_r = 2\pi 0.9722 \frac{c}{D}$$

First radial mode (n = 0):

$$\frac{p}{p_{max}} = J_0\left(\frac{\omega_r r}{c}\right) \cos \omega\tau$$

$$\omega = \omega_r = 2\pi 1.2197 \frac{c}{D}$$

In order to obtain the first spinning tangential mode, two first standing tangential modes at the same amplitude, 90° apart and 90° out of phase, must be combined:

$$J_1\left(\frac{\omega_r r}{c}\right)\cos\omega_r\tau\cos\zeta + J_1\left(\frac{\omega_r r}{c}\right)\cos\left(\omega_r\tau+\frac{\pi}{2}\right)\cos\left(\zeta+\frac{\pi}{2}\right) = J_1\left(\frac{\omega_r r}{c}\right)\cos\left(\omega_r\tau+\zeta\right)$$

If a longitudinal transverse combination is tested, the resonant frequency is

$$f = \left(\frac{1}{2\pi}\right)\sqrt{\omega_z^2+\omega_r^2}$$

$$\omega_z = \frac{2\pi mc}{2\ell}$$

where ℓ is the chamber longitudinal dimension.

The instantaneous pressure profiles for the modes used in the experiment are given in figure 33.

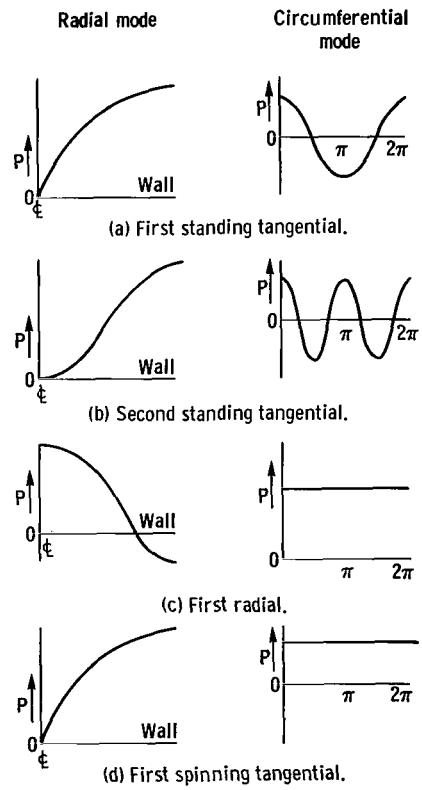

Figure 33. - Instantaneous pressure profiles of acoustic modes tested.

APPENDIX D

FREQUENCY-SHIFT THEORY

The acoustic potential for a cylindrical cavity is defined by

$$\psi = \cos n\zeta \cos \frac{\omega_z Z}{c} \cos \omega\tau J_n\left(\frac{\omega_r r}{c}\right) \tag{D1}$$

This expression is obtained from the wave equation in cylindrical coordinates by separation of variables. The terms ω_z and ω_r are defined by the boundary conditions at the end of the cavity and at the walls, respectively. For a rigid solid wall, the boundary condition is defined for the cavity ends by

$$\frac{\partial}{\partial z}\left(\cos \frac{\omega_z Z}{c}\right)\Bigg|_{Z=0,\ell} = 0 \tag{D2}$$

and for the cavity walls by

$$\frac{\partial}{\partial r}\left(J_n \frac{\omega_r r}{c}\right)\Bigg|_{r=R} = 0 \tag{D3}$$

A physical interpretation of the boundary conditions is that the acoustic particle velocity into the wall or end is zero.

For absorbing walls, equation (D3) is no longer true. Therefore, another means of determining the cavity resonant frequency must be found. The means chosen to determine the frequencies is the technique of boundary perturbations given in reference 10. If no longitudinal modes are to be considered, the angular resonant frequency is defined by ω_r. Therefore,

$$\omega_n = \omega_r \tag{D4}$$

The expression for the shifted resonant frequency of the n^{th} transverse mode is given in reference 10 (pp. 410-412) by

$$\omega_r = \omega_{on} - \frac{\bar{c}\bar{S}_I}{2\bar{V}_I} \tag{D5}$$

where ω_{on} is the unshifted resonance frequency of the n^{th} transverse mode,

$$\bar{S}_I = \int\int \psi^2 \gamma d \text{ (surface area of cavity)} \tag{D6}$$

$$\bar{V}_I = \int\int\int \psi^2 d \text{ (volume of cavity)} \tag{D7}$$

The term γ is defined as the imaginary part of the admittance of the cavity wall Y, where

$$Y = \frac{1}{Z} = \frac{\theta}{\theta^2 + X^2} + \frac{iX}{\theta^2 + X^2} \tag{D8}$$

But

$$Y = \eta - i\gamma \tag{D9}$$

Therefore,

$$\gamma = \frac{-X}{\theta^2 + X^2} \tag{D10}$$

It should be recalled that

See errata

$$X = \frac{2\pi f_0 \ell_{eff}}{c\sigma\theta}\left(\frac{f}{f_0} - \frac{f_0}{f}\right) \tag{D11}$$

If $f > f_0$, X is positive; if $f < f_0$, X is negative. If X is $\pm$, γ is $\mp$ and if γ is $\mp$ and $\bar{S}_I$ is $\mp$, then

$$\omega_n \gtrless \omega_{on}$$

Hence, if $f > f_0$, then $\omega_n > \omega_{on}$ or the resonant frequency of the cavity increases. This would have the effect of shifting the chamber resonance frequencies away from the liner resonance frequency.

REFERENCES

1. Ross, C. C.; and Datner, P.: A Monograph on the Problem of Combustion Instability in Liquid-Propellant Rocket Motors. Paper No. 181-54, ARS, 1954.

2. Fox, Jerome L.: Preliminary Investigation of Helmholtz Resonators for Damping Pressure Fluctuations in 3.6-Inch Ram-Jet at Mach Number 1.9. NACA RM E51C05, 1951.

3. Ingard, Uno: On the Theory and Design of Acoustic Resonators. Acoustical Soc. Am. J., vol. 25, no. 6, Nov. 1953, pp. 1037-1061.

4. Blackman, A. W.: Effect of Nonlinear Losses on the Design of Absorbers for Combustion Instabilities. ARS J., vol. 30, no. 11, Nov. 1960, pp. 1022-1028.

5. Mechel, F.; Mertens, P.; and Schilz, W.: Research on Sound Propagation in Sound-Absorbent Ducts with Superimposed Air Streams. Final Rep. (AMRL-TDR-62-140, vols. I, II, and III), Physikalisches Inst., Univ. Göttingen, West Germany, Dec. 1962.

6. Olynyk, D.; Northwood, T. D.: Comparison of Reverberation-Room and Impedance-Tube Absorption Measurements. Acoustical Soc. Am. J., vol. 36, no. 11, Nov. 1964, pp. 2171-2174.

7. Wieber, Paul R.: Acoustic Decay Coefficients of Simulated Rocket Combustors. NASA TN D-3425, 1966.

8. Hunt, Frederick V.: Investigation of Room Acoustics by Steady-State Transmission Measurements. I. Acoustical Soc. Am. J., vol. 10, no. 3, Jan. 1939, pp. 216-227.

9. Beranek, Leo L.: Noise Reduction. McGraw-Hill Book Company, Inc., 1960.

10. Morse, Philip M.: Vibration and Sound. Second ed., McGraw-Hill Book Co., Inc., 1948.

11. Zwikker, C.; and Kosten, C. W.: Sound Absorbing Materials. Elsevier Publishing Co., Inc., 1949.

12. McAuliffe, Clinton E.: The Influence of High-Speed Air Flow on the Behavior of Acoustical Elements. M. Sc. Thesis., Mass. Instit. Tech., 1950.

"The aeronautical and space activities of the United States shall be conducted so as to contribute . . . to the expansion of human knowledge of phenomena in the atmosphere and space. The Administration shall provide for the widest practicable and appropriate dissemination of information concerning its activities and the results thereof."

—NATIONAL AERONAUTICS AND SPACE ACT OF 1958

NASA SCIENTIFIC AND TECHNICAL PUBLICATIONS

TECHNICAL REPORTS: Scientific and technical information considered important, complete, and a lasting contribution to existing knowledge.

TECHNICAL NOTES: Information less broad in scope but nevertheless of importance as a contribution to existing knowledge.

TECHNICAL MEMORANDUMS: Information receiving limited distribution because of preliminary data, security classification, or other reasons.

CONTRACTOR REPORTS: Technical information generated in connection with a NASA contract or grant and released under NASA auspices.

TECHNICAL TRANSLATIONS: Information published in a foreign language considered to merit NASA distribution in English.

TECHNICAL REPRINTS: Information derived from NASA activities and initially published in the form of journal articles.

SPECIAL PUBLICATIONS: Information derived from or of value to NASA activities but not necessarily reporting the results of individual NASA-programmed scientific efforts. Publications include conference proceedings, monographs, data compilations, handbooks, sourcebooks, and special bibliographies.

Details on the availability of these publications may be obtained from:

SCIENTIFIC AND TECHNICAL INFORMATION DIVISION

NATIONAL AERONAUTICS AND SPACE ADMINISTRATION

Washington, D.C. 20546